Enhanced Biomechanical Characteristics of Connective Tissues and Development of Artificial Implants

Ph.D. thesis

RNDr. Ferdinand Varga

Charles University in Prague

2nd Faculty of Medicine

Department of Biophysics

field of study: Medical Biophysics

supervisor: doc. RNDr. Evžen Amler, CSc.

Prague 2009

Acknowledgements

First of all, I would like to express my gratitude to my supervisor doc. RNDr. Evžen Amler, CSc. for acquainting me with the presented topic, as well as for his suggestions and progressive attitude.

Further, my many thanks belong to RNDr. Milan Držík, Ph.D. and Mgr. Juraj Chlpík, Ph.D. from International Laser Center, Bratislava and Mgr. Vladimír Držík for their substantial contribution to development of presented experimental methods.

I would like to thank RNDr. Ladislav Jirsa, Ph.D. from Institute of Information Theory and Automation, Czech Academy of Sciences for his scientific and philosophic guidance.

My many thanks belong to my colleagues RNDr. Petr Heřman, RNDr. Lucie Koláčná, Ph.D. and Ing. Hana Pokorná from the Department of Biophysics, 2nd Medical Faculty of Charles University for their inevitable help and support. Essential was as well collaboration with Mgr. Eva Filová, Ph.D., Mgr. Michala Rampichová and others from the Laboratory of Tissue Engineering, Institute of Experimental Medicine, Czech Academy of Sciences, for which I am also very thankful. I cherish necessary support of doc. MUDr. Milan Handl, Ph.D. and MUDr. Petr Kos from Orthopaedic Department, Faculty Hospital Motol. Thanks for contribution in data processing belong to Ing. Václav Chudáček from Department of Cybernetics, Czech Technical University. Appreciated is also cooperation of all not mentioned involved specialist.

I am enormously grateful to my family and friends for their help and support.

I would like to express here also my tribute and enduring memory of doc. MUDr. Tomáš Blažek, CSc. and doc. Jindřiška Heřmanská, CSc.

Contents

List of abbreviations

ACI	autologous chondrocyte implantation
ACL	anterior cruciate ligament
GAG	glycosaminoglycan
HA	hyaluronic acid
LDV	laser Doppler vibrometer
PAM	piezoelectric accelerometer
PBTB	bone-patellar tendon-bone ligament
PG	proteoglycan

Summary

Hyaline cartilages are designed to enable smooth life-long articular movement. They serve also substantial role in load bearing, being loaded especially in normal compression. Eventual deterioration of articular cartilage tissue therefore has crucial consequences for affected individual. Characterization of native articular cartilage and application of gained knowledge in reconstructive cartilage treatment is therefore desired. Mechanical characteristics are of prime importance.

Blunt impact testing method in pendulum setup was developed to characterize cartilage tissue under physiological values of dynamic compressive loading. Information on impact process was simultaneously read by piezoelectric accelerometer and laser doppler vibrometer. Acquired data were processed to form loading diagrams and to evaluate standard mechanical quantities. The method was found to be consistent, reliable and effective way of mechanical characterization.

Introduced technique was used for qualitative and quantitative description of native articular cartilage, correlation of its condition with mechanical properties, assessment of tissue engineered materials quality and approval of newly designed artificial materials suitability. Considering native cartilage status, dissipated energy was found to be the most sensitive mechanical marker of its degradation. In tissue engineered materials, different approaches were confirmed to improve their mechanical properties. Analogous experimental system was set for dynamic tensile testing. It was employed in comparative study of knee anterior cruciate ligament and grafts used for its transplantation.

1 Introduction

1.1 Characteristics of articular cartilages and their role in organism

Hyaline cartilage, the most common type of cartilage in the human body, is an essential component in enabling free joint movement. This attribute is due to its low-friction and low-wear properties. It also constitutes a substantial elastic and damping component of the musculoskeletal system. Cartilaginous tissue is composed of chondrocytes and extracellular matrix. As cartilage is an avascular and alymphatic tissue, nutrition of mature chondrocytes must be provided by synovial fluid. Three types of cartilage can be found in human organism: hyaline cartilage (most common, forms articular surfaces), elastic cartilage (present in auricles, epiglottis, Eustachian tube etc.) and fibrocartilage (e.g. intervertebral discs).

Biomechanics of cartilage and other load-bearing materials are of prime importance as they enable and execute body mechanics. Structural failure of hyaline cartilage is closely associated with the mechanical properties of the essential cartilage substances. Maintaining the mechanical integrity of the hyaline cartilage surface is therefore highly important. Excessive force on joints, applied beyond the mechanical tolerance of constituent tissues, should therefore be avoided [1].

Mechanical features of cartilage are mainly conditioned by extracellular matrix constitution. Hyaline cartilage matrix consists of type II collagen (approximately 60 % of dry weight), proteoglycans (25 %) and other proteins and glycoproteins (15 %) [2, 3]. Of the aforementioned particulates, proteoglycans (PGs) and other proteins are the binding components of amorphous extracellular substances. All components of extracellular matrix are synthesized by chondrocytes and subsequently organized into highly structured framework. Chondrocytes form less then 10 % of dry cartilage weight [4] and 5 % of overall tissue volume [5]. Water contributes to approximately 80 % of articular cartilage weight. It serves as a solvent and transport medium. Maintenance of this high percentage is due to interactions between water and the structural macromolecules present in the cartilage. The structure of hyaline cartilage, whose spatial orientation varies throughout the cartilage layers, consists of arcades of collagen fibers that are formed vertically from the subchondral bone, arching beneath and finally running parallel to the cartilage surface. The superficial cartilage zone is richest in chodrocytes. Collagen arcades firmly bind the hydrated cartilage matrix to the underlying subchondral bone. Cartilage failure follows the softening, fibrillation and disruption of this structure. The final result of such degradation is a full-thickness defect of the cartilage surface with loss of matrix constituents [6]. The ability to self-repair is extremely lim-

ited as there is no blood supply and relatively few cells are available to fully restore the damaged structure.

Impairment of joints can lead to loss of mobility and sense of pain. Most common causes are sprains, ligament ruptures, full-thickness defects and derangement of articular hyaline cartilage. Numerous surgical procedures have been developed for the treatment of damaged hyaline cartilage, but until now there has been no evidence of long-term restoration of full-thickness defects [7, 8]. According to the literature, less than 5 % of the 500 000 hyaline cartilage defects diagnosed in 2001 were treated with one of the repair techniques [9]. Autologous cultured chondrocytes as a hyaline-like cartilage in the form of a solid chondrograft (fixed by fibrin glue) become now more popular and frequent as one of several possible procedures used for reconstructing full-thickness chondral lesions of joints, mostly in the knee [10].

Practical need of joint cartilage properties determination results from efforts for cartilage degenerative diseases early diagnosing and treatment. Articular cartilage failure often leads to osteoarthritis. It has been suggested that joint injuries and mechanical overload during heavy manual labor may be among the frequent precipitating causes of such failure [11]. Osteoarthritis and rheumatoid arthritis are the most frequent joint diseases. They are of different etiology but share similar feature: progressive degradation of articular cartilage that leads to joint dysfunction. In both pathologies, erosion of the cartilage matrix is thought to appear primarily due to increased synthesis and activation of proteinases involved in the degenerative process. Cartilage breakdown due to disease results in severe pain and disability. Except for the commonly performed conservative and operative therapy, a new approach has recently appeared – implantation of autologous chondrocytes grown on a suitable scaffold support [12, 13]. Science of implants and tissue engineering calls for proper mechanical characterization of native cartilages, as resemblance to the original tissue properties is required.

1.2 Tissue engineering in cartilage impairments treatment

Tissue engineering is a modern approach in therapy of articular cartilage diseases. Chondrocytes embedded in biocompatible three-dimensional scaffolds preferably composed of biodegradable polymers, such as collagen, fibrin, polyglycolic acid, polylactic acid, hyaluronic acid etc., are reported as a novel attitude to cartilage repair [14, 15]. In routine human medicine fibrin scaffolds are commonly used for the past decade [16] and their enhancement is continuously carried out. Biodegradable artificial scaffolds should support chondrocyte proliferation and nutrition, improve their re-differentiation capacity and provide them with an appropriate mechanical stability.

Particular scaffold designed for chondrocyte cultivation has to meet several major

requirements, such as biocompatibility, adequate degree of biodegredability and proper mechanical characteristics. Implantation of material that is too stiff will result in its emphasized load-bearing function and imbalance in pressure distribution inside the joint. This may lead to early implant destruction or even to severe joint structure deterioration. Implant structure that is too soft will most probably result in reduced chances for its integration in surrounding cartilage tissue, as the implant will be loaded nonphysiologically mostly sideways and not normally. Both the mentioned situations will substantially worsen the after-surgery convalescence and rehabilitation or even cause complete implant rejection. To avoid such complications, proper biomechanical properties of engineered and implanted cartilage substitutes are again essential [17].

1.3 Physiological loading of articular cartilages

Water makes up majority of native cartilage mass and it plays principal role in ability of the tissue to withstand large compressive forces. Solid cartilage structures are thus exposed to hydrostatic pressure. In diarthroidal joints this interstitial pressure ranges between 5–10 MPa and it is applied periodically during normal activities [2, 4]. The human hip and knee joint may sustain loads up to ten times body weight, which may rise up to 18 MPa of compressive stress [2, 5].

Considering loading dynamics, during normal gait acting force rises to peak in approximately 100 ms [18]. Corresponding typical loads in tibio-femoral joint are about two to three times body weight, loading rates of order of 20 $kN.s^{-1}$ and strain rates of the order of 5 s^{-1} [19]. During running loading time shortens to about 30 ms, acting forces are about 2 kN and loading rate of order of 200 $kN.s^{-1}$ [20].

Articular cartilage is able to withstand wide range of applied stresses, depending especially on its condition and applied strain-rate. For impact loading accepted critical stress value causing chondrocytes death and ruptures in extracellular matrix is 15–20 MPa [21, 22]. Recently measured ultimate stress values causing irreversible damage of articular cartilage in impact testing range from 16 to 237 MPa depending on impact energy and strain-rate applied [23, 24].

1.4 Articular cartilage composition related to its mechanical function

As explained above (section 1.1), articular cartilage consists of two distinct phases: solid and fluid one. Solid phase consists mainly of chondrcytes, collagen fibers, proteoglycans and other glycoproteins. Chondrocytes are responsible for cartilage tissue metabolic activity, formation and degradation of extracellular matrix. They as well

exert a contractile force on attached extracellular matrix components, being partially responsible for passive tension within the tissue and active tensile response to external stress [25]. Superficial articular cartilage zone, which is richest in chondrocytes, is thus the one exhibiting substantial internal tension, causing curling of cartilage removed from underlying bone [26]. The solid matrix is filled with interstitial fluid, forming the fluid phase of cartilage structure.

1.4.1 Extracellular matrix of articular cartilage

Collagen content is also highest in the surface zone and decreases with depth, proteoglycan content is inversely related. Collagen polypeptide chains coiled into left handed helices form tropocollagen units consisting of three chains screwed into right-handed helix. Tropocollagen of type II collagen then builds up fibers of 20–200 nm diameter and varying length [2]. Collagen network is then facilitated by covalent cross-links between the collagen molecules, providing high tensile stiffness and strength for the tissue.

Proteoglycans (PGs) are composed of protein core with attached glycosaminoglycan (GAG) chains. PG monomers bind to hyaluronic acid monofilament chain to form an aggregate. The GAG chains of PGs provide important physico-chemical properties to cartilage, due to their ionization. Negatively charged chains determine presence of positively charged ions in the interstitial fluid (mainly Na^+) via the Donnan equilibrium. This ion concentration governs the osmotic pressure ranging from 0.1 to 0.2 MPa, contributing up to 50 % of cartilage compressive stiffness [27]. Repulsive forces between charged chains along with the osmotic pressure between interstitial fluid and external solution help to maintain extracellular matrix stretched and inflated, causing cartilage swelling. Furthermore, PGs exhibit networking capability, which stabilizes extracellular matrix. Non-covalent (electrostatic and mechanical) interactions exist also between collagen and PG molecules (Fig. 1). In this way, collagen network provides tensile stiffness and strength, while PG network provides the compressive stiffness of extracellular matrix [2].

1.4.2 Contribution of interstitial fluid to cartilage mechanical properties

Extracellular matrix forms pores with diameter ranging from 2 to 6 nm [28]. These pores are occupied by water – forming the fluid phase of cartilage tissue. Minor portion of water occupies space within collagen fibers – these water molecules are not free to move. Tiny pores of extracellular matrix also form an effective barrier for larger molecules. Interstitial fluid thus consist mainly of water and dissolved ions and exhibits Newtonian fluid properties. Water content variations reflect those of collagen, being

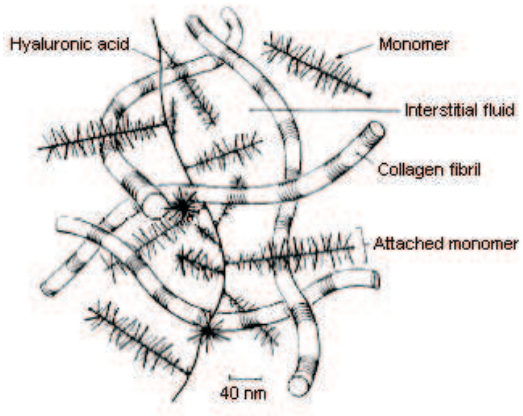

Figure 1: The collagen network interacting with proteoglycan network in cartilage extracellular matrix. Proteoglycan monomers composed of protein core and glycosaminoglycan chains bound to hyaluronic acid molecule [2].

highest at the cartilage surface and decreasing with depth. The majority of water molecules exists in the solution domain of PGs, when charge of PG chains is the most important factor in determining the amount of water present. Organization and material properties of collagen-proteoglycan matrix affect the amount of water present as well. Under compressive or tensile stress water molecules flow through the nano-scaled matrix pores, ensuring stress distribution. Frictional interactions between the water molecules and walls of pores substantially determine mechanical properties of cartilage tissue, being a dominant mechanism of cartilage viscoelastic behaviour under compression. The matrix permeability for present fluid is highly dependent on compressive strain and applied pressure; with increasing compressive strain or pressure the permeability decreases [2]. Generally very low permeability of cartilage matrix to fluid flow gives rise to high fluid pressure and high drag forces between the fluid and the matrix during interstitial fluid flow [29]. The fluid pressurization provides the dominant mechanism for load bearing of joint cartilage. Along with energy dissipation generated mainly through solid-fluid interactions it provides an efficient shield to cartilage matrix during loading.

1.4.3 Viscoelastic and poroelastic properties of articular cartilage

The described cartilage composition determines its viscoelastic properties. There are three principal differences in mechanical response between viscoelastic and elastic material [30]: (i) Mechanical response of viscoelastic material depends on time. A dependence on strain rate is present – the faster is the deformation, the larger stress is required. Under constant loading further strain develops – this phenomenon is called creep of the material. (ii) The loading and unloading curves do not coincide, but form

a hysteresis loop. Considering the loading diagram, area beneath the loading curve represents energy stored in the material while during unloading it is the energy recovered. Their difference, area of the hysteresis loop, thus equals to the energy lost mainly through heat transfer. (iii) Permanent deformations may appear upon complete unloading, also postponed recovery of materials original size and capabilities after some time is possible.

Further phenomenon worth mentioning is a phase angle (phase lag) characterizing how much behind is the actual response of strain value compared to instant stress applied (ranges from 0° for ideally elastic material to 90° in totally plastic one). It is subjected to energy losses during the loading process. This feature, also typical for cartilage tissue, is characteristic for poroelastic materials and sometimes understood as a principal difference between poroelastic and viscoelastic substance. Thus, articular cartilage is also often regarded as poroelastic [31].

1.5 Evaluation of cartilage mechanical properties in compressive testing

Poroelastic nature of cartilage tissue implies that the mechanical parameters such as stiffness or elastic modulus and viscoelastic characteristics are highly strain rate dependent [32]. Suitable mechanical characterization is therefore rather complicated and it seems to be one of the principal limitations of broader application of tissue-engineering in cartilage repair.

1.5.1 Quasi-static vs. dynamic testing methods

Recently, the cartilage mechanical properties have been mostly evaluated by both static and dynamic tests. Different strain rate (the "velocity of deformation") is usually understood as the principal difference between the quasi-static and dynamic measurement mode. Due to the specific nature of articular cartilage, compressive forces are usually applied in its examination.

Measurements are usually conducted via loading test on universal testing machines [33–36]. There is a vast variety of commercially available testing devices allowing mechanical material testing in compression, tension, shear, torsion, flexure, fatigue, examining its hardness or ductility. Samples are usually attached between two grips or clamps. Conventional testing approaches involve the constant load, constant load-rate, and constant displacement-rate. As these modalities are quite ordinary in general material testing, they are as well most common for evaluation of cartilage tissue mechanical properties. However, this kind of testing is mainly appropriate to low

strain rate conditions and the data obtained have thus a limited value. Moreover, in quasi-static conditions also material creep is significant.

In order to extend the possibilities of biological material testing, several measuring procedures based on cyclic loading have been proposed [37,38]. Nevertheless, also such a testing abounds in evaluation difficulties due to the impossibility of avoiding fluid escape from solid matrix when larger strains are applied. Furthermore, after each cycle of compression loading a considerable residual compression arises whereby the slope of the loading curve (material stiffness) is increasing cycle by cycle, making thus difficult to define the basic parameters of the material [39]. In quasi-static testing the material's continuous adjustment to applied pressure is supposed, unlike in dynamic testing, when changes are too fast to adapt to. The material's response is different when different strain rates are used [40].

1.5.2 Indentation testing methods

Indentation techniques [41–43] for compressive cartilage testing gained major attention recently. As few hand-held indentation probes have been designed [44, 45], this approach has been brought a further step closer to practical cartilage quality assessment. Operating part of indentation probe is usually formed by approximately 5 mm diameter stainless steel rod/tube with tip customized for indentation purposes and with controlled application of loading force [44, 46] or ended by a vibration unit consisting of compliant oscillating beam in cantilever configuration for dynamic measurements [45]. Indentation techniques generally examine certain sample segment, which is surrounded by its natural environment (i.e. surrounding cartilage tissue). Non-indenting techniques usually deal with samples in unconfined loading, which affects their mechanical performance. Substantial benefit of indentation probes is that they can function arthroscopically. Quantities like stiffness and shear modulus have been evaluated in cartilage characterization using indentation probes in referenced studies. Although the technique is relatively simple in principle, the quantitative interpretation of experimental data is not always straightforward. Technique thus suits mainly needs of comparative experiments, not objective quantitative evaluation. Available manufactured indentation probes usually provide measurement in device-specific relative scale [42, 47] or Newtons of applied force [46, 48].

Indentation principle has been extended to further dimensions. Suh et al. [49] introduced use of miniature ultrasound transducer as a mechanical indentation probe, while exploiting emitted ultrasound wave for cartilage thickness measurement. Lu et al. [50] indented cartilage samples by water jet with ultrasound beam propagating inside the water flow. Knowing the applied pressure, deformation was read utilizing

ultrasound echo.

Micro- and nanoindentation are today well established methods for examination of mechanical parameters of biological materials, especially bone, dentin and cartilage, as well as their developed substitutes (e.g. [51–56]). Tip sizes used for indentation ensure that the indentation area is usually of a few square micrometers or even nanometers. Analogous principle is utilized in employing scanning probe microscopy devices for indentation purposes, bringing advantage of high-resolution surface characterization (e.g. [57,58]). As nanoindentors provide by default loading curves as an output, variety of mechanical characteristics can be evaluated. Among them reduced modulus is the most common. In native cartilage characterization some operating difficulties appear, conditioned mainly by sample uneven surface. In return, measurements are extremely precise and capable to determine mechanical properties of individual tissue components on cellular and subcellular level. Such a characterization is obviously very valuable for tissue engineering purposes.

1.5.3 Alternative testing methods

Less frequent are studies employing other alternative approaches. Hattori et al. [59], Kuroki et al. [60] and others evaluated echo duration and maximum magnitude in diagnostic frequency ultrasound examination and found those specific for different grades of cartilage alteration as gained in macroscopic classification. Berkenblit et al. [61] applied small sinusoidal currents to the surface of articular cartilage to measure current-generated stress. Sachs et al. [62] used electromechanical spectroscopy to model response of cartilage subjected to a periodic mechanical displacement applied to the articular surface. They found this nondestructive method able to detect focal regions of cartilage degeneration. Dashefsky [63] utilized constructed microminiature pressure transducer to qualitatively assess chondromalacia of patellar facet under arthroscopic control.

1.5.4 Impact testing methods

For a large range of strain rates and loading mechanisms applied in introduced mechanical examinations of articular cartilage there could be found a physiological argument. These tests will though never cover the whole extent of physiologically possible loading of the joint cartilage. On the other hand, the so-called impact loading of joint cartilages is often a neglected feature of exceptional physiological meaning. Within the impact loading mode, applied force continuously decreases along with the strain rate. The impact is damped and its energy partially dissipated regarding material properties. This process, lasting only a few milliseconds, is natural also for articular cartilage

loading *in vivo* – especially in the bearing joints. The fact that the cartilage response to such stimulation is not sufficiently described yet can be partly attributed to the lack of adequate methods and commercially available equipment.

In order to better understand the real dynamic behavior of the material, several attempts have been made to measure and simulate the impact loading stress state. However, while a lot of studies have been devoted to numerical modeling of stress/strain generated in articular cartilage under such loading conditions [22, 64, 65] only a limited number of experiments analyzed and characterized comprehensively basic material parameters [21]. The early measurement methods in the so-called drop-tower design [21, 66] could not estimate the descending part of the loading curve, thus evaluating the energy dissipation and determination of ultimate strength were hindered. Most common setup of these experiments up to now is that the specimen placed on an anvil is struck by a free falling mass of impactor lead by guiding rods ("free falling" when neglecting the friction). In the "drop-tower" experiments it was difficult to control the peak force at which the test specimen first exceeds the elastic limit. It appears also problematic to locate and characterize the first signs of failure and determine if they occur in the subchondral bone or in the cartilage itself. Enhanced drop-tower apparatus [19, 67] has recently been used especially to examine effects of shock loading on cartilage. This design enables modification of loading rate (velocity) and energy by means of controlled impact employing different masses and drop heights. Piezoelectric force transducer and accelerometer were used to yield information about deformation process. Critical mechanical characteristics such as maximum dynamic modulus, maximum stiffness, stress and strain have been evaluated using this approach. These were further compared to quasi-static characteristics [23]. Preliminary results on dissipated energy values and effect of underlying substrate were as well presented. Analogous experimental design was used to evaluate storage modulus and absorbed energy [24]. Available impact testing studies are in fact exclusively focused on critical impact loading of cartilage, examining its survival capacities and thus using very high strain rates (approximately 500–1500 s^{-1}). Mechanical behaviour of articular cartilage under conditions of physiological dynamics is still neglected. In the "drop-tower" setup, though recently enhanced and utilized as described, the unloading phase of impact process is rather questionable, as gravity acts against sample reaction. Probably, the lack of abundant experimental information and more extensive cartilage characterization is caused also by technical problems with the realization of measurements and interpretation of acquired data. Therefore, the method for impact characterization of cartilage tissue using blunt impact was desired.

Impact testing in material science is ordinarily performed by Charpy and Izod tests. Both of them use a swinging pendulum mass to attack the sample (differ in sample

positioning) and measure the energy absorbed by a standard notched specimen while breaking under an impact load. The idea of this setup has not been yet used, according to our knowledge, for characterization of biological samples. Still, it appears potentially helpful in overcoming many of the lacks of above mentioned testing methods.

Articular cartilage is most definitely not stressed only in compression. Most of acting forces in diarthroidal joints act in direction normal to the cartilage surface causing cartilage compression. Nevertheless, joint movement causes also tensile and shear stresses within articular cartilage. Tensile and shear cartilage characteristics are thus also extensively studied (e.g. [22, 29, 36, 68, 69]).

1.6 Role of tensile dynamic testing in reconstructive surgery of ligaments

In contrary to mainly compressively loaded cartilages, ligaments and tendons are components of musculoskeletal system loaded mostly in tension. Ligaments and tendons consist mostly of aligned collagen fibers, which thus crucially determine their mechanical properties. Tissue engineering approach in reconstructive medicine of tendons and ligament is yet not established, mainly because of extreme mechanical demands and impossibility of partial substitution. Therefore reconstruction using autologous grafts is still the only practically feasible treatment possibility. Relevance of mechanical properties of used graft, when compared to the original tissue, is here obviously as well of prime importance. Available tension tests are in principle mostly analogous to universal testing machines in compressive setup. Dynamic tests again play a principal role due to nature of physiological loading.

Anterior cruciate ligament reconstuction is the most common one among substitutive surgeries of ligaments and tendons. Biomechanical properties of the graft material are the critical factor in success of such reconstructions [70–73]. Most of the reconstruction techniques describe different grafts and fixation methods [74]; other studies have been conducted to compare the biomechanical properties of different grafts [75]. Most previous studies of graft materials were focused on their elastic and failure properties [38], especially their ultimate load and stiffness.

1.7 Relations of biomechanical and clinical cartilage condition characteristics

Mechanical characterization, though extensively developed, does not serve yet for cartilage diagnosing. Standard diagnostic techniques for hyaline articular cartilage condition assessment nowadays employ macroscopic observations based on X-ray, CT, NMR

or arthroscopic imaging. These approaches are somewhat subjective and expect macroscopic tissue alteration. Nowadays, expertize techniques based on mentioned imaging modalities are being developed to facilitate their evidence based quantitative interpretation [76–79]. Microscopic histological examinations are more objective, but as well more time demanding and necessitate bioptic tissue sampling. In X-rays Outerbridge scoring is usually used and the most common arthroscopic evaluations follow the ICRS scoring schedule based on Outerbridge score [80]. The most frequently used scoring systems for histopathological examination has been as well set by the ICRS [81] and proposed by Mankin [82].

Referring to animal experiments [83,84], significant relation of cartilage biomechanical features with degree of their structural alteration on histopathological level would be expected. Biomechanical properties of human articular cartilage have been extensively studied so far, but not many of the studies correlating these results to the clinical examinations can be found [85]. Elastic modulus usually serves as a representative mechanical characteristic in such research. Even more rare are studies relating dynamic mechanical properties with histopathology [69]. Measurement of mechanical cartilage parameters in situ has been already pioneered [46], being a promising alternative approach in cartilage diagnosing. As already mentioned, indentation instruments that could be used for such purposes have been designed and tested (e.g. [44, 45, 47]).

Mutual comparison of mechanical and clinical examination would give a deeper insight into the processes of pathological cartilage deterioration as well as its consequences. Furthermore, development of a minimally invasive technique for *in vivo* measurement of cartilage mechanical properties could help more effective early diagnosing of eventual impairment. Thoroughly designed classification of cartilage mechanics in different stages of deterioration would be essential for such a diagnostic feature. This can be suggested, as alteration in biomechanical properties can be notable before any gross morphological change is apparent [86, 87].

1.8 Demands on experimental setup, biomechanical data and their analysis

As it is apparent, each of listed methods for cartilage compressive mechanical testing faces several limitations. Quasi-static testing on well tuned and precise commercially available devices faces problems with applying higher strain rates as well as handling specific samples of interest. Dynamic tests usually apply frequencies higher than physiological. Drop-tower impact testing is partially limited in determining sample recovery and has been so far used as well exclusively for high strain rates. Indentation techniques are very promising, especially as they are in principle enabling *in vivo* mea-

surements. Still they often lack objective evaluation of measured data absolute values. Nanoindentation is another fine and precise technique, but again facing problems with examination of native-shaped samples. Further, it is very valuable for material characterization in micro-scale, but gained information is then rather distant from general macroscopic mechanical tissue properties.

The key problems of a comprehensive evaluation of the cartilage mechanical parameters are the necessity of dynamic testing over a large range of strain rates along with the requirement for sensitive acquisition and correct interpretation of highly nonlinear testing data. Moreover, characteristics of available biological samples have to be taken into account when designing experimental setup. Usually only small volume specimens are available: they are moist, greasy and slippery, suffer drying and fade away with aging, they are of irregular shape and uneven surface and possess anisotropic properties. Some of the standardized, commercially available testing machines deal with specific features of biological specimens and can thus be used for compression as well as tension testing under certain restrictions. Limitations, unfortunately, are often very serious. Several laboratories have attempted to overcome these limitations at least partially [36, 38, 39, 88, 89].

As both the native and tissue engineered cartilage material have a complex poroelastic and anisotropic structure, their description by only simple characteristic value (e.g. Young's modulus or Poisson's ratio) is, thus, definitely not satisfactory for adequate evaluation and comparison of their biomechanical properties. Furthermore, it may result in the development of unsuitable implants. Other problematic points include the comprehensive characterization of anisotropy of biological material [64, 90] and the Poisson's ratio [91, 92], which are indispensable for numerical modeling.

Major differences in mechanical properties between the implant and the surrounding original tissue would naturally hamper the implant-integration process and may lead to its rejection or disruption. As a more suitable and valuable characterization of nonlinear material, compared to above mentioned characteristics of linearly elastic materials, appears a stress-strain diagram. Loading diagrams in form of force-displacement or stress-strain relation are quite common outputs of mechanical loading tests. Information involved in such a diagram is rather complex and calls for description and analysis, essential for its further practical employment. Diagram characterizing features of certain biomechanical meaning and medical relevance are thus in pursuit.

In exploratory data analysis it is common to use methods such as creation of decision trees [93] to discover rules hidden in the data itself. Here, extraction of characteristic features is motivated by two different goals. Firstly, it is wanted to find out mathematical features that would describe the curves precisely, while maintaining their general information value. Secondly, it is demanded to extract features with biomechanical

meaning, such as dissipation energy, tangent modulus etc. Comparison of their performance with respect to the newly proposed curve-descriptive features would follow. Most suitable and efficient features can then be utilized for automatized, data-driven cartilage classification.

1.9 Goals of the study

1) The crucial aim of the study was to develop reliable mechanical testing method overcoming several of the limitations of available techniques. Our main concerns were:

(i) Avoiding problems caused by nature of tested samples, their shape, size and consistency. This requires customized sample attachment and proper and well defined applying of the loading force.

(ii) Enabling specimens characterization under loading conditions resembling physiological loading (strain-rate, applied energies and stresses).

(iii) Focusing on uniaxial compressive loading from macroscopic point of view. This approach was regarded as the most simple, most predicative and most useful for comparative studies, concerning materials of different origin.

(iv) Making the method as much effective as possible, easy to handle and bringing high information yield. Unbiased loading diagrams were the desired output.

(v) Developing a methodology for processing of the achieved information and for evaluation of characteristic quantities.

Further objectives dealt with practical employment of proposed testing method:

2) Application of designed method for comprehensive characterization of native articular cartilage tissue.

3) Mechanical characterization of tissue-engineered materials and their comparison to native tissue.

4) Advanced characterization of both the native and artificial cartilage. Concerning native cartilage, this would basically mean distinguishing healthy and damaged tissue. Considering artificial tissue, progressive enhancement of materials developed as scaffolds for autologous chondrocytes implantations was of interest.

5) Correlation of revealed mechanical properties of native articular cartilage with results of standard diagnostic procedures. Assess possibilities of employing mechanical testing as another diagnostic tool.

2 Methods and materials

2.1 Theoretical model of cartilage impact testing

Considering mechanical element impact testing, material response to higher rates of loading is evaluated applying force pulse. One of the simplest designs is the drop-test technique, where a body of specified weight impacts the tested specimen. The shape and duration of the shock pulse is determined by the colliding materials intrinsic characteristics, the shape of colliding surfaces and the original drop-weight position and mass (i.e. the energy of impact). The required conditions of loading, thus, can be determined by a proper drop-weigh impact velocity and the mass of impacting hammer.

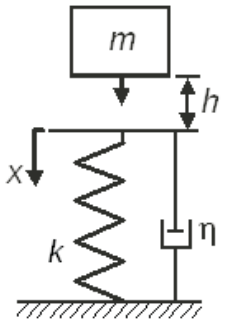

Figure 2: Scheme of testing apparatus and tested sample (m – mass of impacting body, h – impact height, x – sample deformation, k – spring constant, η - viscoelastic damping constant).

The tested cartilage element can be resembled in simplified model by a spring and a parallel damper representing viscoelastic damping of the material (Fig. 2). The spring end motion during drop-weight impact can be described as

$$\ddot{x} + 2\kappa\dot{x} + \omega_{\mathrm{E}}^2 x + \omega_{\mathrm{P}}^2 x^2 = g \tag{1}$$

where

$$\omega_{\mathrm{E}} = \sqrt{\frac{k_0}{m}}, \quad \omega_{\mathrm{P}} = \sqrt{\frac{\xi}{m}}, \quad \kappa = \frac{\eta}{2m}$$

while m is the impacting mass; g is acceleration due to gravity; x is deformation, η is the constant of material viscoelastic damping, k_0 is the constant spring value, ξ is the coefficient of non-linearity and $k(x) = k_0 + \xi x$ is the spring element stiffness. We have assumed the bearing element as a hardening spring in equation (1). As a first approximation, its stiffness rises linearly with the deformation. Then, the force of spring deformation can be expressed as

$$F = -k(x)x \tag{2}$$

with the boundary conditions

$$x = 0$$

$$\dot{x} = v = \sqrt{2gh} \quad \text{at} \quad t = 0 \tag{3}$$
$$F(0) = \eta\sqrt{2gh} \quad \text{at} \quad t = 0$$

where h is the drop height (difference between the original and the very bottom impactor position).

The required information on loading force vs. time and/or specimen deformation vs. time can be determined by detecting the time dependent signal of a drop-weight acceleration/deceleration. Alternatively it can be done tracking its velocity during the impact. The development of instantaneous displacement after the impact initiation can be regarded as an elongation/compression of the element tested. The time dependence of impacting mass acceleration identifies loading force. As the mass of drop-weight is constant, the loading force during impact follows from the Newton's force law

$$F = ma \tag{4}$$

Based on Eq. (1) a simple numerical model of the impact process can be created, including simulation of viscoelasticity and stiffness non-linearity. For linear elastic material where the stiffness k is proportional to the constant value of Young's modulus $E(\xi = 0)$, the damping factor η can be neglected and we obtain a linear loading diagram. In order to simulate genuine articular cartilage element, the parameters have to be chosen near to their actual values.

For better resembling of the situation, entering values of the impact velocity $v = 0.05$–0.08 ms^{-1}, inertial mass $m = 0.545$ kg and stiffness corresponding to that of cartilage materials revealed in experiments were used. Fig. 3 shows simulated loading diagram with the hysteresis loop.

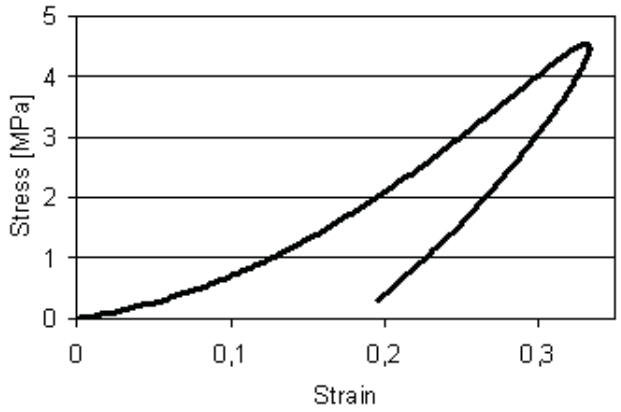

Figure 3: Shape of the dynamic loading diagram as it was simulated numerically.

The loading curve in this case considerably differs from that of linear course; after starting with low slope the cartilage element becomes stiffer. Further course is influ-

enced by viscoelastic compliance. If the loading force does not exceed the ultimate strength of element, hysteresis curve will occur.

2.2 Blunt impact compressive testing method in pendulum setup

2.2.1 Instrumentation

The impact testing procedure has been realized by a simple lab-designed pendulum-like drop-test apparatus. The method makes use of a continuous measurement of striking mass deceleration/acceleration and velocity in time. The impact process is conditioned by dimensions of the tested specimen as well as by its mechanical parameters. In an attempt to secure easy handling, good measurement reproducibility and avoiding unwanted disturbing forces, a steel pendulum was manufactured. Its leg was 30 cm long, mass was 0.545 kg and circular contact area diameter was $\phi = 5.5$ mm (Fig. 4). The amplitude of acting force and the impact energy have been set by a suitable initial height of pendulum striking body. Impacting pendulum weight was interchangeable as well.

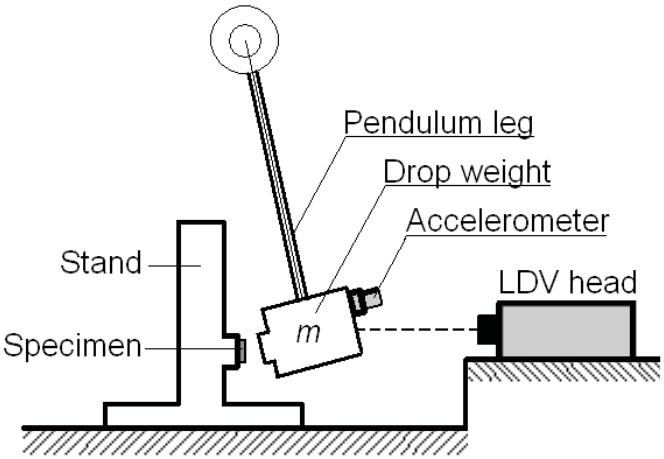

Figure 4: Scheme of experimental setup for cartilage impact testing.

2.2.2 Data acquisition

The proposed process tracking is based on the use of piezoelectric accelerometer (PAM) and contactless sensing by Laser Doppler Vibrometer (LDV). Continual reading of the time traces of velocity or acceleration during the impact provides all the information required to determine the loading force, acting stress as well as tested specimen deformation (compression). When dealing with small, very thin samples and relatively low

dynamic loads, such approach seems to be desirable. Therefore, the head of the pendulum was equipped with a firmly attached piezoelectric accelerometer Bruel & Kjaer Type 4375. Producer recommends this PAM type for tracking of impact processes. Its weight is 2.4 g, resonance frequency 73 kHz and sensitivity 0.314 pC/ms^{-2}. Obtained signal was amplified by a preamplifier Robotron RFT 00 042, charge amplifier Bruel & Kjaer Type 2525 and recorded by Tektronics TDS 220 digital oscilloscope. A care was taken when using PAM sensors to detect transient processes. Nevertheless, the rates of measured accelerations were too low in comparison with the natural vibrations of the sensor.

The measurement is not limited by the sample size, as far as the original thickness and contact area of the sample with the striking body are determined. The accelerometer is able to reliably read displacements in order of 10^{-6} m. Therefore use of accelerometer relieves the problem that is often the case, when small volume specimens are only available for testing.

For contactless reading the heterodyne Polytec LDV with an OFV-302 interferometric head and an OFV-2601 controller was installed. Its laser beam was aimed at the posterior side of the pendulum hammer to measure pendulum velocity. Even though the LDV is intended as a tool for measuring vibrations, its working principle allows the sensor to be used to detect velocity variations in single-event shock pulses. The main purpose for the installation of LDV and thus duplicating the accelerometer measurement was to check mutually both of the detected signals and enable well-founded data processing, as described below. In the experiments performed, the impact velocities of the impinging weight did not exceed 1.5 ms^{-1} and thus stayed well within the LDV controller's measurement range.

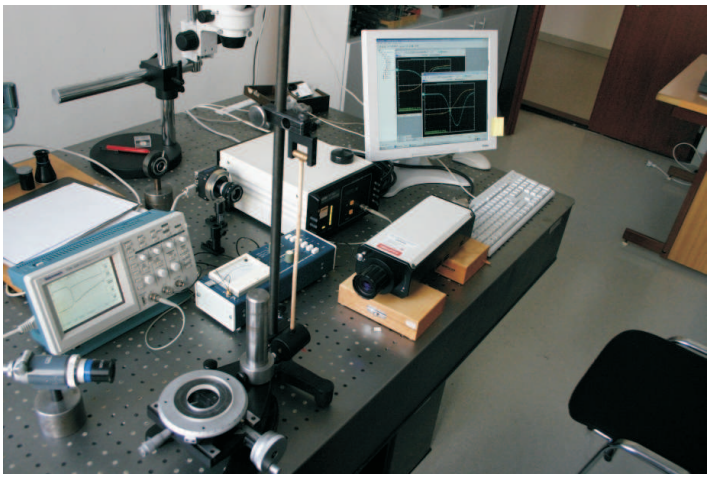

Figure 5: Realization of experimental setup for cartilage impact testing – general view.

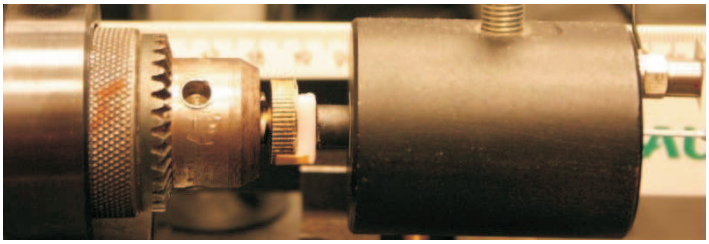

Figure 6: Realization of experimental setup for cartilage impact testing – detail (chondrograft sample adhering on the stand anvil).

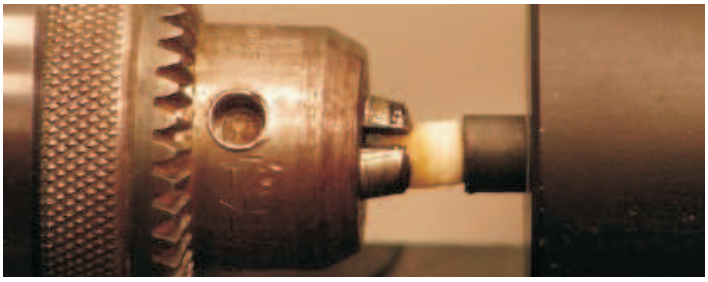

Figure 7: Realization of experimental setup for cartilage impact testing - detail (cartilage-on-bone sample attached in chucking appliance of the stand).

The records obtained by both PAM and LDV detectors coincide mutually very well. It can be ascertained by numerical integration or differentiation processing (in Fig. 8 integration of PAM signal was performed to achieve velocity values). Fig. 8 shows time course of the signals as they were recorded with one of the cartilage specimens, using both detectors. There is an opportunity to use any of the two detectors independently, once thoroughly calibrated.

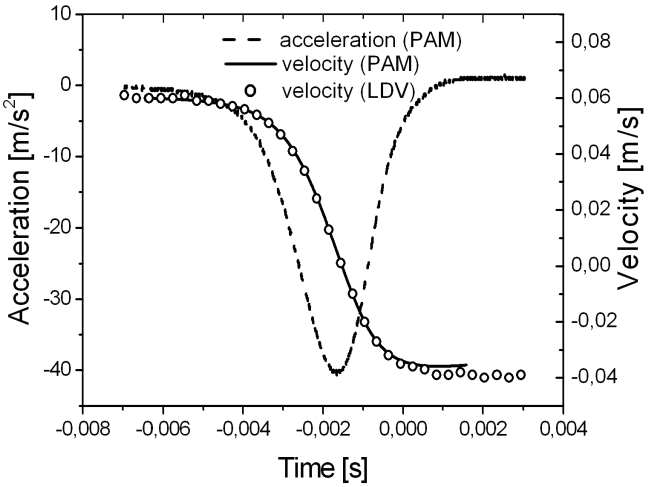

Figure 8: Examples of the recorded acceleration (PAM) and velocity (LDV) signals. Velocity time course obtained by PAM signal time integration is presented as "velocity (PAM)".

2.2.3 Measurement parameters

To perform the experiment, the pendulum struck specimen positioned horizontally, with surface perpendicular to the hammer motion. The pendulum was released from defined height to assure desired impact energy and it was stopped after its bounce. In joint cartilage loading, an impact is considered to be dynamic force application on or behind the border of physiological values. To specify cartilage impact loading following values are respected: acting forces reach their maximum in less then 50 ms after contact, loading rate is 100 $kN.s^{-1}$ or higher, stress rate is greater than 1000 $MPa.s^{-1}$ or strain rate is greater than 500 s^{-1} [20, 32]. These values are generally presumed to cause cartilage injuries. Physiological loading values were mentioned in introduction section (1.3, p. 9). For the experiments performed in this study, loading resembling physiological one was used rather than recommended extreme values. Impact velocities used for different experiments ranged from 0.05 to 0.3 $m.s^{-1}$, resulting in strain rates in order of 1 s^{-1} and 10 s^{-1}. Achieved maximal stresses ranged approximately from 1 MPa to 20 MPa. These intervals were found to be appropriate for description of physiological cartilage response as well as for finding the ultimate values in cartilage loading.

Tested specimens were attached to fixed steel stand serving as a vertical anvil. They were mounted in a manner respecting their nature. Native and tissue engineered cartilage samples were, if possible, kept in the testing position solely by adhesion. Once they were not adhering (knitted material, dry material etc.), an adhesive tape was used. Cartilage-on-bone samples were clamped in a chucking appliance, maintaining full cartilage thickness unconstrained (Figs. 6 and 7). Neither the stand nor the adhesive tape on interface contributed to measured response and thus did not affect the resulting signal.

2.2.4 Data processing

The pendulum hammer deceleration/acceleration signal was preconditioned and recorded. Double time integration of the deceleration/acceleration signal has been performed to acquire the history of the specimen's instantaneous deformation:

$$\Delta l = \int_{t_1}^{t_2} \left(\int_{t_1}^{t_2} a(t) \mathrm{d}t \right) \mathrm{d}t \tag{5}$$

where Δl is the elongation, t_1 and t_2 are the time integral boundaries denoting the initiation and termination of concerned signal, respectively.

LDV has served for determination of impactor velocity, namely for determination

of initial velocity v_1 required in integration procedure (eq. 5).

$$v(t) + v_1 = \int a(t)\mathrm{d}t$$

Integration constant v_1 was identified as an initial velocity of impactor at the time of its contact with the specimen.

The defined elongation Δl (eq. 5) related to original specimen thickness l was considered as the strain ε:

$$\varepsilon = \frac{\Delta l}{l} \tag{6}$$

Stress σ was evaluated as ratio of the actual acting force F (proportional to acceleration a, (eq. 4)) and contact area (S):

$$\sigma = \frac{ma}{S} \tag{7}$$

where m is the pendulum head mass.

In such manner all the quantities required for setting up the loading diagrams can be evaluated – acting force and actual deformation as well as compressive stress and actual strain. An application in LabView environment has been developed for described data processing and force-displacement curves composition (Fig. 9).

In further data analysis, virtual preload was considered prior to the impact process. In practice – the initial part of loading diagram was cut off up to stated force value (usually 1 N). This should partially resemble physiological load at rest. Main reason for introducing the virtual preload was to unify identification of the starting point of the loading diagram, suppressing substantial uncertainty.

In uniaxial loading tests, stiffness and elasticity modulus are usually used to quantify the mechanical properties of the specimen. As examined material exhibits nonlinear properties, tangential (differential) stiffness k and modulus Θ have to be considered. For this sake measured diagrams had to be approximated by smooth curves. Cubic regression (polynomial fitting of 3$^{\mathrm{rd}}$ order) appeared accurate enough in majority of cases ($p < 0.0001$). These fits were then used in analytical form to evaluate tangential quantities as follows:

$$k = \frac{\mathrm{d}F}{\mathrm{d}l} \quad [\mathrm{N.m^{-1}}] \tag{8}$$

$$\Theta = \frac{\mathrm{d}\sigma}{\mathrm{d}\varepsilon} \quad [\mathrm{Pa}] \tag{9}$$

Precise deformation velocity (loading mass movement velocity) evaluation enables energy balance interpretation. The overall energy of impact E_1 can be considered equal

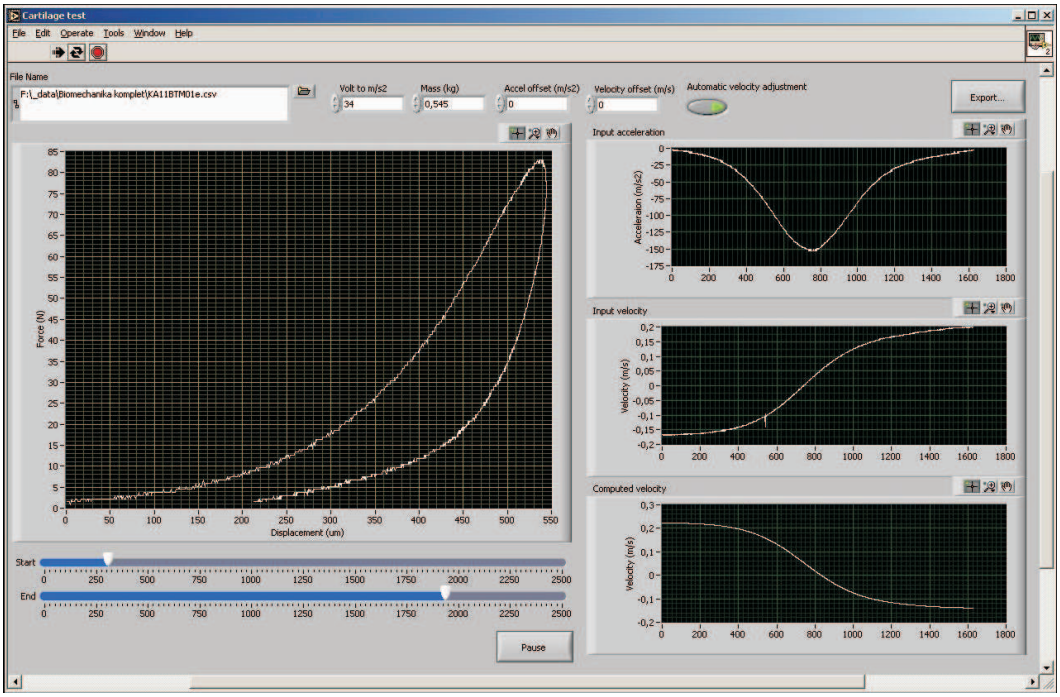

Figure 9: Screenshot of application for raw data processing.

to kinetic energy of striking body just before (or at the very moment of) its contact with the sample:

$$E_1 = \int_0^{l_{\max}} F_1(l)\mathrm{d}l = \frac{1}{2} m {v_1}^2 \tag{10}$$

where $l_{\max}$ is maximal deformation of the sample, F_1 is force acting during the sample compression and v_1 is the velocity of striking body at the instant of the first contact. The area under ascending part of the loading diagram curve graphically represents the impact energy E_1 as defined by eq. (10).

The mechanical energy lost within the process of deformation – dissipated energy ΔE – can then be evaluated as the difference between kinetic energy of the striking body at the very beginning E_1 and very end E_2 of the deformation process. This is graphically represented by the area under the whole loading curve – the hysteresis loop (Fig. 10):

$$\Delta E = E_1 - E_2 = \int_0^{l_{\max}} F_1(l)\mathrm{d}l - \int_{l_{\max}}^{0} F_2(l)\mathrm{d}l = \frac{1}{2} m {v_1}^2 - \frac{1}{2} m {v_2}^2 \tag{11}$$

where v_1 is again initial striking body velocity, v_2 is the velocity of striking body just rebounded, F_1 is force acting during the compressive part of impact process – ascending curve, while F_2 force during reaction (decompression) phase – descending curve. In other words, dissipated energy is a difference between stored (E_1) and restituted (E_2) energy.

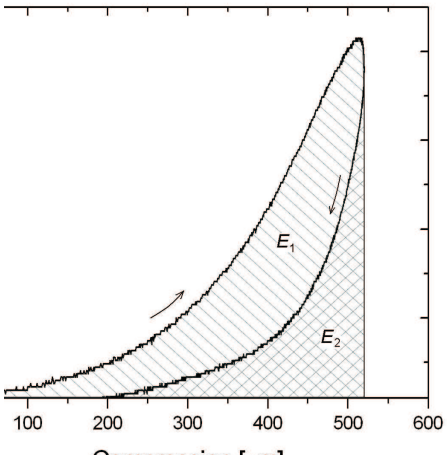

Figure 10: Experimentally achieved loading diagram illustrating impact energy balance. Total stored energy of impact denoted E_1 and restituted energy (F_2), their difference – area of hysteresis – represents the dissipated energy.

Based on the evaluation of integrals (11), further quantities characterizing energy loss can be evaluated. Normalized dissipated energy per unit volume ΔE_{N} should enable comparison of intrinsic characteristics of individual cartilage samples:

$$\Delta E_{\mathrm{N}} = \frac{\Delta E}{V} \tag{12}$$

where V is sample volume. Specific damping capacity (or absorbed energy ratio) is a material characteristic defined as:

$$\Psi = \frac{\Delta E}{E_1} \tag{13}$$

Most of the calculations and data processing were carried out in Microcal Origin software.

2.2.5 Comparative standard quasi-static mechanical testing

The quasi-static loading of the tested specimen was realized to confront the results obtained by the proposed impulse testing methodology with those measured using standard universal device. Commercial testing machine MTC 858.2 Mini Bionix was used for this purpose. Two different strain rates were applied: 5 mm.min^{-1} and 10 mm.min^{-1}.

2.3 Impact tensile testing

Analogous principle in appropriately modified setup can be employed for tensile dynamic testing. Tendons and ligaments are musculoskeletal system components loaded mainly in tension, therefore their tensile properties are of interest. The method is based

on a rapid increase in the loading force, creating a subsequent elongation of the tendon element up to its failure. By measuring the time-dependent signal of the drop-weight velocity or alternatively its acceleration, the required information is yielded. Loading force vs. time, drop-weight energy vs. time and the tested specimen's elongation vs. time can be extracted this way. The schematic drawing of the shock testing in Fig. 2 can be applied in this situation as well.

In order to realize the proposed impact test, a simple drop-test apparatus was manufactured. The bearing structure is a frame where one end of the test specimen is fixed (Fig. 11). Specially designed clamps were used to avoid soft tissue slippage or failure caused by stress at the clamp-tendon interface. The fixation clamps were wedge-shaped grips of steel with rough surfaces on the contact faces. A sandpaper interface was introduced to reduce the stress concentration as well as to prevent the tendon from slipping out of the clamp-holder. These clamps allow the tissues to be adequately held without affecting the point of significant damage. A small vertical shift of the sliding jaws couple inside the flat conical guiding spacer, which is initiated by the tensile force, presses the grips and the fixed tendon end against each other. Identical conical grips are used at the lower end of tendon specimen, where a movable lightweight rigid frame is suspended. The impact force of the falling weight is transferred to the specimen by means of the suspended frame. When examining the doubled or quadrupled specimens, one end of the graft strands (or double loop) was mounted into the superior end of the testing machine. The upper clamp fixed either the free-, the looped- tendon or the bone-end samples. The lower clamp fixed the free tendon or the bone ends. The distance between the edges of the grips could be varied from 30 mm to 80 mm. Such a simply-conceived test machine brings advantageous possibility to vary both the drop height and mass of the striker, thus creating different loading/strain rates and also varying the total amount of impact energy.

Experimental data were achieved and processed analogously to compressive impact testing method. Piezoelectric accelerometer correlated with the proper apparatus was again employed, together with a Laser Doppler Vibrometer for contactless measurement of movable suspended frame motion. From experimental experience, the application of a vibrometer system has proved to be preferable to standard piezoelectric accelerometers with regards to the superior suppression of high-frequency acceleration noise. The raw signals of both the acceleration and velocity were recorded in digital form by a two-channel oscilloscope. Subsequently, the records were transferred to a PC and processed by numerical integration and/or differentiation. The view of the apparatus depicted in Fig. 12 shows the suspension of the movable frame on a tendon specimen.

As can be seen in Fig. 13, the transmission of kinetic energy to the system is accompanied by a certain ripple superimposed upon the test pulse, resulting from the natural

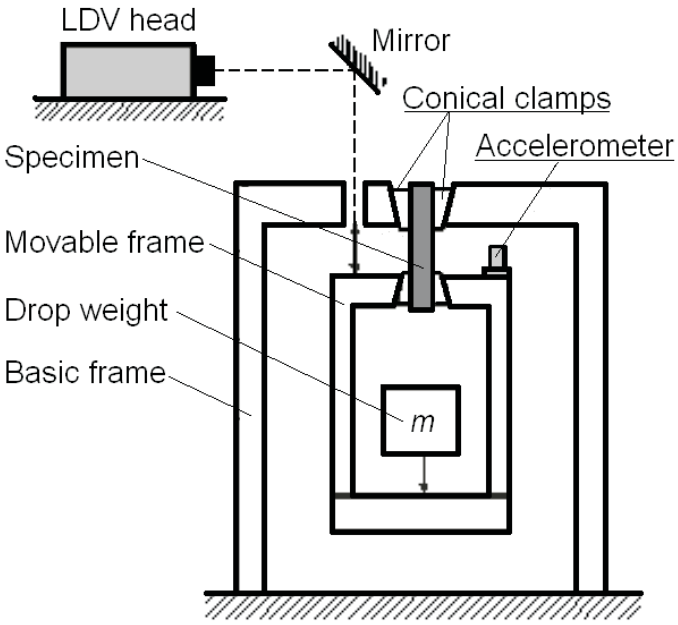

Figure 11: Scheme of experimental setup of drop-test apparatus for dynamic loading of tendons.

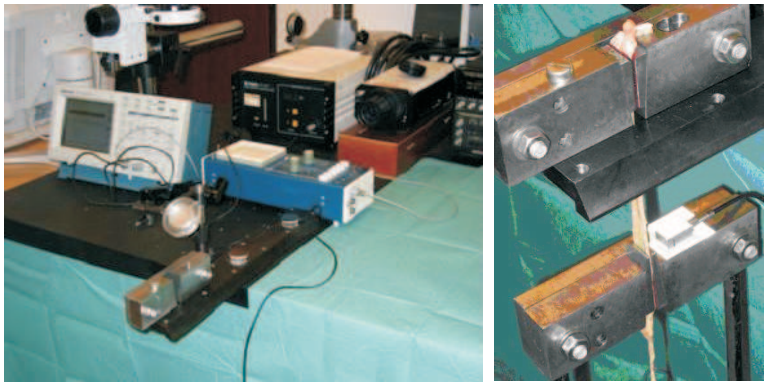

Figure 12: General view of the measurement apparatus and a tendon specimen suspended on movable frame with clamps.

vibration of the testing frame. This rippling effect can be avoided either by appropriate mechanical damping or by reprocessing the original sensor signal by a suitable numerical smoothing. As the signals were differentiated to obtain the decellerating force development, cubic splines interpolation proved to be an adequate procedure. Fig. 13 shows an illustrative example of the time trace of the movable specimen jaw. The signal was recorded by the LDV in one of the conducted experiments. The graph also shows the curve of specimen elongation as obtained by numerical integration.

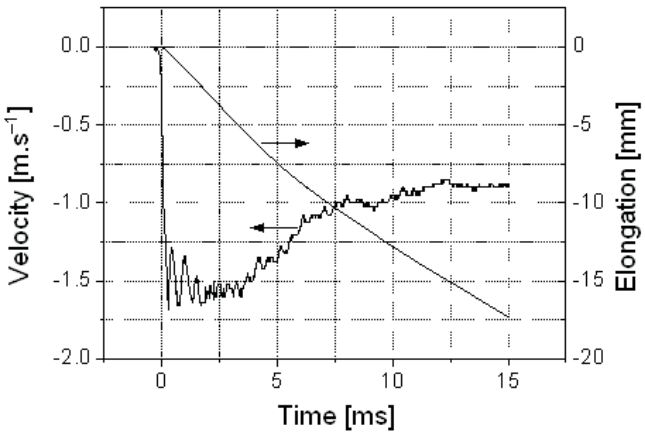

Figure 13: One of the recorded velocity traces with evaluated elongation course for a gracilis tendon specimen.

2.4 Samples preparation

All samples of biological origin were obtained respecting ethical codex. Presented experiments were branches of officially approved projects. Most of the samples were leftovers in experimental or routine surgical procedures.

2.4.1 Pig knee cartilage samples for verification measurements

Cylindrical cartilage plugs with 5 mm diameter were tested. Samples have been prepared from mini pig knee cartilages, harvested and treated as described in [94]. Each sample was shaped planparallel, with the thickness ranging from 0.6 to 1.7 mm. Samples were loaded in direction normal to original cartilage surface. No animals were exploited solely for these testing purposes, the samples used were leftovers within parallel experiments, though fresh and intact.

2.4.2 Tissue-engineered scaffolds and chondrografts for *in vivo* and *in vitro* studies

Small pieces of cartilage were taken under general anesthesia from the rabbit left femoral trochlea [95]. After 14 hours of digestion in collagenase solution, the chondrocytes were collected and cultured for 14 days supplemented with fetal bovine serum and growth factors. The cells were incubated at 37 °C in 5 % CO_2 atmosphere. Scaffold was prepared of hyaluronan and type I collagen, then it was combined with cell suspension and further growth factors. Tissucol and trombine solutions (Tissucol Kit, Baxter AG, Austria) were then added to the mixture. Then the scaffold was placed into the incubator for one more day. Four different scaffolds (six pieces of each) were

produced, differing in volume of hyaluronan and collagen used (see Tab. 1). Fibrin scaffold without hyaluronan and collagen was prepared as well.

Scaffold	**Cell Suspension** [μl]	**HA** [μl]	**Collagen** [μl]	**Tissuecol** [ml]	**Trombin** [ml]
1	40	12.5	18.8	0.06	0.06
2	40	16.25	13.6	0.06	0.06
3	40	8.75	24.4	0.06	0.06
4	40	0	0	0.09	0.09

Table 1: Scaffolds with variable volume of hyaluronan (HA), type I collagen, Tissucol and Trombin and chondrocyte suspension.

Knitted textile scaffolds were tested as well. Presented are results for Chirlac knitted matrices. Chirlac threads are composed of polyglycolic acid fibres with 150 μm diameter. The material is biodegradable and routinely used in surgical sewing. Scaffolds were hand-knitted, with diameter of 6 mm and thickness ranging from 2 to 3 mm.

2.4.3 Human native and tissue-engineered cartilages for mechanical characterization in uniaxial dynamic compression

Hyaline cartilage samples were harvested from 18 operated human knee joints and served as the source material for chondrograft preparation and biomechanical testing. In all patients were excluded previous metabolic, general bone and other pathologies of the knee joint. The mean donor age was 30.45 years, with a range of 19 to 44 years.

All cartilage samples were exploited solely for mechanical testing and chondocytes culturing purposes. The samples used were fresh and intact leftovers from the regular surgical procedure or samples from the non-weight bearing zone of the articular surface. Special harvesting cutting tubes of 2 mm diameter were employed to provide the same shape and size of samples tested. In general, five different types of samples were used for this study's purposes. Sample 1 derives from the non-weight bearing zone of the trochlea femoris (in fact a healthy cartilage), while sample 2 is from the center of the full-thickness defect zone. Sample 3, respectively sample 4 were finally formed into solid fibrin chondrografts Type 1 (slow solidification process) and the upgraded Type 2 version (controlled rate solidification process). Such grafts are used in routine medical practice for autologous chondorocyte implantations. Sample 5 – Type 3 chondrograft was a tested, newly designed chondrograft based on fibrin scaffold, enriched with collagen and hyaluronic acid. In all cases the solid chondrografts were obtained after *in vitro* cultivation of autologous chondrocytes over a period of approximately 28 days. Process of cell cultivation and chondrograft preparation was analogous to the one described in previous paragraph (section 2.4.2).

Preparation of chondrografts

The basic procedure of combining the chondrocytes with the carrier matrix was the same for all three of the grafts. The fibrin glue (Tissuecol Kit, Baxter) was prepared according to instructions. Fibrinogen and aprotinin were mixed with thrombin and calcium ions to form the fibrin glue. Types 1 and 2 differ in the way the mixtures were treated after the chondrocytes had been added to the fibrin glue. With chondrograft Type 1, the solidification process proceeded spontaneously at a room temperature of 21°C, without any external interference. After approximately two hours the final solid form was achieved. With chondrograft Type 2, the solidification process was controlled by gradually lowering the temperature from 30 to 15°C over a 30-minute period. Matrix forming into the chondrograft was stored in a firmly closed plastic container and kept in a water bath, which resulted in a denser product. Type 3 chondrograft contained hyaluronic acid, type I collagen, fibrin and chondrocytes as Scaffold 1 specified in previous paragraph (section 2.4.2, Tab. 1, according to [95]) but without growth factors.

2.4.4 Human articular cartilages for correlation of mechanical characteristics with histological and macroscopical classification

For the purpose of this study, 120 articular cartilage samples were harvested from 15 patients knees. Donors were of average age 72.2 years (range 57–84 years). Samples were dissected from remaining tissue at total knee joint replacement surgeries, using special harvesting tube. From each joint 4 pairs of corresponding adjacent plugs were harvested. Each of the sample pair came from different location: femoral lateral condyle, femoral medial condyle, tibial lateral condyle and tibial medial condyle. All the sample plugs were 6 mm in diameter and contained a layer of subchondral bone. Thickness of cartilage layer ranged from 0.6 to 4.2 mm. One sample of each pair (i.e. total of 60 samples) was examined histologically and its condition evaluated according to ICRS histological score ([81], specified in Tab. 2). Corresponding sample form each harvested pair was examined macroscopically and scored according to ICRS macroscopic score ([96], specified in Tab. 4). Further it was examined for its mechanical properties. Cartilage thickness was measured digitally from samples photographs shot prior to mechanical testing.

Histological classification of samples

Samples for histological evaluation were of complete cartilage thickness with clear orientation. Decalcinated formalin-fixed tissue samples were parafin-embedded. Histological slides were stained using hematoxylin-eosin.

For improper or not available histological or biomechanical data 9 of the harvested

cartilage samples pairs were excluded from the study, thus 51 sample pairs were involved. Samples were categorized into 4 groups according to histological findings following ICRS classification schedule (Tab. 2), regarding severity of damage histologically approved. Criteria listed in Tab. 3 were chosen as the most reasonable in the available set of samples.

Feature	**Score**	**No. of samples**
I Surface		
smooth / continuous	3	15
discontinuities / irregularities	0	36
II Matrix		
hyaline	3	30
mixture: hyaline / fibrocartilage	2	21
fibrocartilage	1	0
fibrous tissue	0	0
III Cell distribution		
columnar	3	6
mixed / columnar-clusters	2	39
clusters	1	6
individual cells / disorganized	0	0
IV Cell population viability		
predominantly viable	3	51
partially viable	1	0
<10% viable	0	0
V Subchondral bone		
normal	3	43
increased remodeling	2	8
bone necrosis / granulation tissue	1	0
detached / fracture / callus at base	0	0
VI Cartilage mineralization (calcified cartilage)		
normal	3	43
abnormal / inappropriate location	0	8

Table 2: Histological classification of cartilages according to ICRS with number of samples fitting individual criteria.

Macroscopic classification of samples

Evaluation of cartilage samples quality according to macroscopic ICRS score is shown in Tab. 4.

Group	Feat. I	Feat. II	Feat. III	Feat. IV	Feat. V	Feat. VI	Total	No. of samples
1	3	2–3	2–3	3	3	3	16–18	15
2	0	3	2	3	3	3	14	14
3	0	2–3	1–2	3	2–3	3	12–13	13
4	0	2–3	1–2	3	2–3	0	9–10	9

Table 3: Categorization of samples according to values reached in individual features of ICRS histological scoring.

ICRS class	Description of cartilage deterioration	No. of samples
0	Normal surface	11
1	Almost normal surface with fibrilation or softening, fissures, cracks	23
2	Abnormal surface - damage up to 50% of cartilage thickness, fraying	19
3	Substantially damaged surface - damaged more than 50% of cartilage thickness, but not up to bone	5
4	Sorely abnormal surface - lesion up to subchondral bone, complete cartilage loss	2

Table 4: Macroscopic classification of cartilages according to ICRS with number of samples fitting individual criteria.

2.4.5 Human ligament and tendon grafts for tensile testing

Fresh-frozen, nonirradiated, unembalmed cadaveric human knees served as the source of graft material. The mean age at death was 67.2 years, with a range of 51–84 years. No signs of bone or soft-tissue injury were found during dissection. The grafts for experiments were obtained from 21 paired knees when 21 pairs of anterior cruciate ligament, bone-patellar tendon-bone, semitendinosus and gracilis tendons were harvested. All cases of previous knee joint surgery, metabolic, bone and other pathologies in the knee region were excluded so that the results would not be distorted. The mean time interval from death to harvesting was 8.7 hrs (range 6–12 hrs). The grafts were obtained bilaterally and treated similarly to surgical procedures with living patients.

3 Results

3.1 Blunt impact testing is a consistent method for retrieval of cartilage tissue characteristics

In pursuit of reliable and effective method for uniaxial dynamic compressive mechanical characterization of specific biological samples, blunt impact method in pendulum setup was developed. The experimental instrumentation, measurement procedure, data acquisition and processing are described in section 2.2.

In preliminary experiments, mechanical behaviour of pig knee cartilages under impact loading was measured. To characterize individual native pig cartilage sample, 5 independent subsequent measurements were processed and the mean value of stress-strain curve was evaluated for each sample. Fig. 14 features resulting curves for single sample and 5 different samples, along with boundaries of 2 standard deviations intervals. Only the ascending part of the diagram, which refers to sample compression during the loading process, is presented.

Derivative of loading diagram represents tangent (or differential elastic) modulus. As Young's modulus in general sense can be considered the derivative of initial, almost-linear part of loading diagram. Even more valuable information about inspected material is brought by maximum stiffness – slope of the loading diagram at the upper extremity.

Considering the tangent modulus as a slope of stress-strain curve (eq. 9, p. 27), its strain dependence can be drawn simply as a derivative of this function. Functional dependence of tangent modulus on actual strain for one of the cartilage samples is shown as inset of Fig. 14.

Fig. 14 thus depicts variance and reproducibility of acquired results.

To describe mechanical response of articular cartilage tissue in compression, quantities like compressive modulus, tangent modulus at certain stress and compressive stiffness are most commonly used. Quite rare is evaluation of dissipated energy or phase angle (lag). All of these quantities are well defined, their evaluation is feasible once suitable data are available. Further important and quite often evaluated features of mechanical performance are survival characteristics of cartilage. An ordinary approach to define these limits is the ultimate (peak, maximum) stress or strength and ultimate strain, that if exceeded the material will fail. Ultimate compressive strength, understood as a minimal acting force causing irreversible change of material, can be assessed using the loading diagram. That would presume irreversible sample deformation by single impact. As the impact velocity (i.e. impact energy) can be gradually

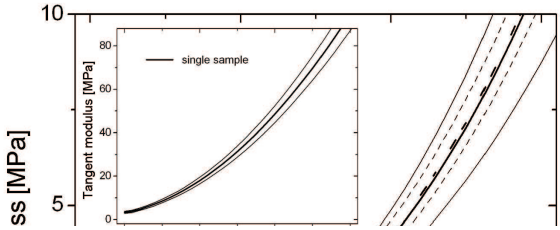

Figure 14: Stress-strain curves of single sample and 5 different samples of native pig joint cartilage, mean values and 2 standard deviations confidence intervals shown. Inset: Tangent modulus nonlinear dependency on actual strain, mean value for single cartilage sample with 2 standard deviations interval shown.

increased and material response monitored, boundary impulse causing irreversible deformation can be extrapolated.

It cannot be said that the material does not experience damage at stresses or strains below the ultimate values. Moreover, the ultimate values are not strictly constant; they are influenced also by strain rate applied. Comparing the higher and lower strain rates of dynamic loading, in the latter case the boundary strain of damage is larger according to our experience. Another important factor is loading repetition rate. This effect is illustrated in Fig. 15. If the recurrence interval lasts seconds or even less the cartilage material is not able to restore its original properties due to incomplete reabsorption of the expelled interstitial fluid in unconfined compression. Then, the cartilage matrix structure is not protected enough for repeated dynamic loads. In such a case the material endurance and resistivity vanish step-by-step even though the impact energy remains at the previous values. In Fig. 15 the impact velocity (i.e. also energy) for last three measurements was almost identical (Fig. 15, curves *c*, *d*, *e*). Despite that the cartilage material gradually degraded from curve *c* through *d* to curve *e*. Time intervals between the impacts were 5–10 seconds at unconfined dynamic compression.

As already mentioned in introduction part, reaction of poroelastic material to static, dynamic and impact loading differs substantially. An example of cartilage biomechanical characteristics comparison obtained by both proposed impact dynamic method and quasi-static loading test using strain rates 5 mm.min^{-1} and 10 mm.min^{-1} is shown in Fig 16.

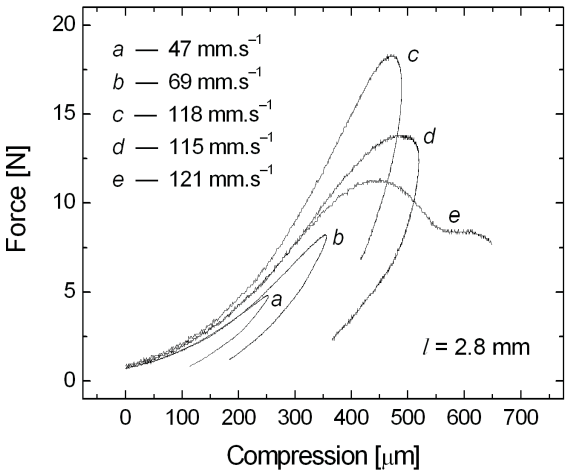

Figure 15: Force-compression loading curves of single hyaline joint cartilage sample – consequent measurements a to e taken in 5–10 s intervals. Initial impact velocities v_1 are denoted for each measurement. Uncompressed sample thickness l = 2.8 mm.

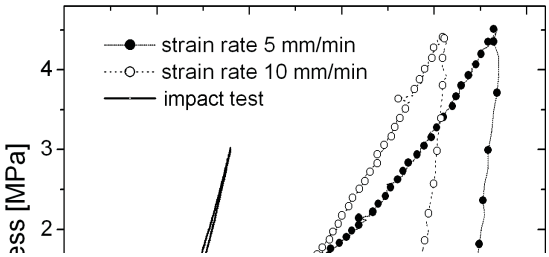

Figure 16: Comparison of single pig articular cartilage sample stress-strain curves for static (strain rate 5 mm.min^{-1} and 10 mm.min^{-1}) and impact test loading.

Cartilage mechanical response to loading stimulus depends quite obviously on loading mode, as seen in Fig. 16. It differs as well with different strain rates in impact loading. Under higher strain rate cartilage appears stiffer, loading diagram is steeper (see Fig. 15). This phenomenon is often referred to as strain-rate-dependent hardening [97].

3.2 Loading diagram achieved in blunt impact testing is an appropriate tool for qualitative comparison of different materials.

As reasoned in introduction section, the loading diagram appears as comprehensive description of non-linear biological material response to dynamic loading – it can either display stress-strain, force-strain or force-deformation relation.

Materials of different mechanical nature exhibit different course of loading diagrams. The ascending (uploading) part of the loading diagram characterizes stiffness of material when being compressed, while the descending part expresses extent of plastic deformation. Ideally elastic, linearly responding material would thus be characterized by a straight line identical for loading and unloading. Majority or real materials exhibit nonlinear characteristics. Viscosity and porosity of material are usually responsible for its nonlinear behaviour. Fig. 17 shows uploading characteristics of different materials, as they were measured using proposed blunt impact testing method.

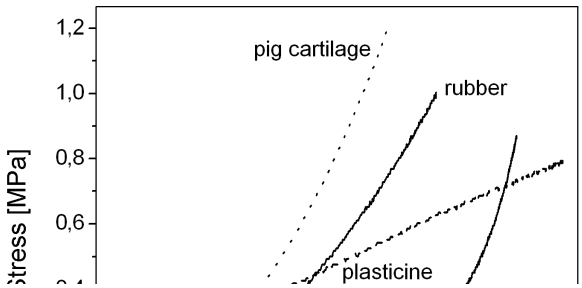

Figure 17: Stress-strain diagrams of different materials as measured in blunt impact testing.

Loading diagram as such allows qualitative comparison of tested samples, even without necessarily evaluating characteristic mechanical quantities. Fig. 18 shows example of native and tissue engineered cartilage comparison. Presented graphs show mean force-deformation curves for native cartilage, fibrin chondrograft used in standardized autologous chondrocyte transplantation surgery, knitted Chirlac fiber matrix in two samples – once only damped in physiological solution and once with chondrocytes after ten days of cultivation. Our results prove insufficient material stiffness (excessive deformation at low acting forces) and higher maximum strain in fibrin chondrograft

sample. Tested Chirlac knitted matrix better resembles course of ascending part of native cartilage loading curve. Chondrocytes cultivated on artificial matrix will affect overall mechanical properties of the material – by forming extracellular network as well as by boosting up scaffold material degradation.

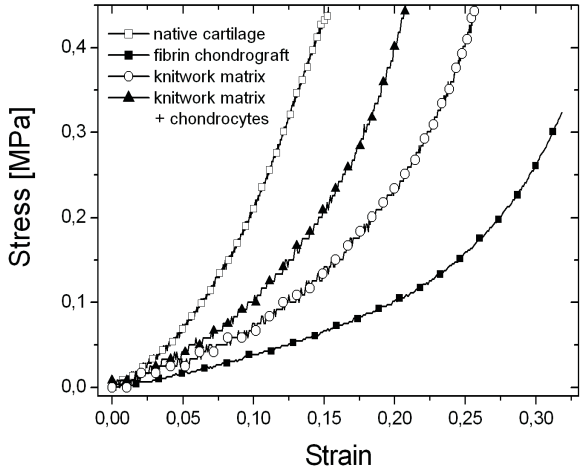

Figure 18: Loading curves of native cartilage and some of the materials tested as scaffolds for tissue engineered cartilage: native human hyaline cartilage sample, fibrin chondrograft used for autologous chondrocyte transplantations, knitted Chirlac fiber matrix – blank damped in physiological solution and same chondrocytes-seeded matrix after a ten-day cultivation.

This qualitative approach was employed in quality assessment of tissue-engineered scaffolds for chondrografts tested in rabbit models [95]. Four proposed scaffold compositions were compared to native cartilage and routinely used fibrin chondrograf. Three of the newly designed structures differed in volume of hyaluronan and collagen involved, while the fourth one was prepared solely from Tissucol and Thrombin (Tab. 1, p. 33). In comparison with fibrin gel, the tested scaffolds exhibited macroscopically higher homogenity, reflecting their higher hydration.

Tested composite matrices demonstrated similar nonlinear course as the native cartilage loading diagram (Fig. 19). Presented results prove that addition of collagen and/or high-molar-mass hyaluronan brought material response closer to the native cartilage. Among the four tested samples, the highest stiffness and mechanical response in general closest to native cartilage were found with Scaffold 1. Therefore it was concluded, that scaffold 1 showed the most convenient biomechanical properties.

One of the characteristic features of the instrumented impact testing based on pendulum type device is the possibility to observe unloading part of force-displacement relationship. Rebound of the impacting mass carries information on material response

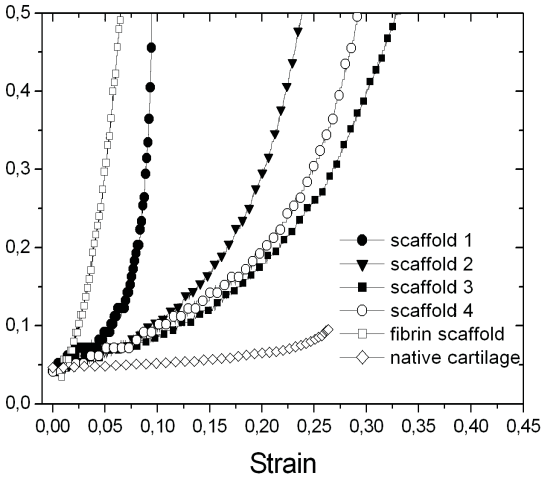

Figure 19: Loading diagrams of different composite scaffolds in comparison to native cartilage. Composition of Scaffolds 1–4 is specified in Tab. 1, p. 33.

to impact, important when analyzing the poroelastic parameters and dynamic mechanical performance. In Fig. 20 complete hysteresis curves examples are shown for the intact human hyaline cartilage tissue and the impaired one. The plotted records of single donor specimens illustrate the differences in shapes and maximum strain values.

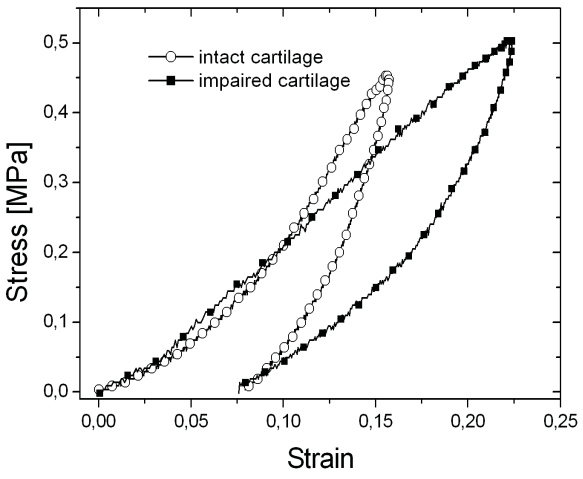

Figure 20: Examples of loading curves for intact human hyaline cartilage tissue from non-weight-bearing zone (sample 1) and cartilage from defect zone (sample 2). "Fibrin scaffold" stands for routinely manufactured and implanted scaffold.

3.3 Mechanical parameters of native and tissue engineered cartilage revealed in blunt impact testing

For the purpose of most common materials characteriaztion a study was ran to evaluate properties of normal and damaged human hyaline cartilage as well as the two types of scaffolds routinely used for autologous chondrocytes transplantation (Type 1 and Type 2 chondrograft). In addition, taking into account previous results, scaffold enriched with collagen was tested as well (Type 3 chondrograft). To characterize individual cartilage and chondrograft samples, five to ten measurements were carried out at different impact energies. Virtual initial preload of 0.5 N was applied at processing of the compression stress-strain diagrams to substitute actual physical preload and to suppress uncertainty in determination of the initial point of the impact. To characterize individual samples, loading diagrams were set. Fig. 21 shows the computer-evaluated force-displacement dependencies of two native cartilage samples from the same subject and collagen enriched chodrograft Type 3. The curves specified here as a‘, b‘, c‘ depict the behaviour of hyaline cartilage from the defect zone, while curves a and b are the intact hyaline cartilages from the non-weight-bearing zone. The curves d, e and f belong to Type 3 chondrograft.

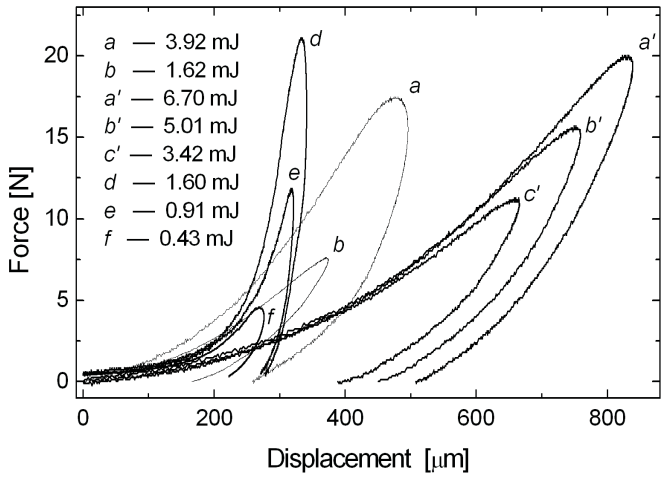

Figure 21: Comparison of the non-weight-bearing zone cartilage force-displacement curve (a, b) with that of the material from the defect zone in the same joint (a', b', c'). The curves (d), (e), (f) belong to collagen-enriched fibrin chondrograft Type 3.

As can be immediately seen from Fig. 21, the material of living human hyaline cartilage shows highly nonlinear behaviour. That is due to the basic composition of the cartilage tissue, where an interstitial fluid saturates the porous solid matrix. The loading process depends on the rate of deformation, hence several force-displacement

dependencies were measured for each of the specimens at different strain rates. During short-duration impact events (20–40 ms) the fluid viscosity controls deformation resistance and prevents tissue from damage. For the cartilage to recover to its initial state, a time interval of 1 to 3 min between impacts was maintained. Thus, due to the elasticity of the solid matrix allowing reabsorption of the exudated fluid, the material recovered its original properties.

Probably the most distinct differences between the three groups of curves shown in Fig. 21 are apparent in mechanical stiffness of the samples. Stiffness is commonly characterized by the slope of linear region of a force-deformation curve, consequently stress-strain relationship determines the modulus of elasticity. Seeing that in the measured loading diagrams no linearly determined material behaviour is present – the tangent modulus has to be defined (eq. 9, p. 27). In Tab. 5 the values of stiffness corresponding to the loading stress $\sigma = 1$ MPa are given along with corresponding values of tangent moduli. Tab. 5 lists also other data of the tested samples from four separate groups of materials: the non-weight-bearing zone, the defect zone and from the Type 1 and Type 2 fibrin based chondrografts with cultured autologous chondrocytes. Two groups of native cartilages were mutually statistically compared – the non-weight-bearing zone with the defect zone and chondrograft Type 1 with Type 2.

	Non-weight bearing zone	**Defect zone**	p	**Type 1 graft**	**Type 2 graft**	p
Ultimate compressive strength [MPa]	11.32 ± 2.32	10.37 ± 4.11	n.s.	7.44 ± 3.98	8.73 ± 4.46	n.s.
Ultimate strain	0.28 ± 0.08	0.30 ± 0.10	n.s.	0.63 ± 0.11	0.57 ± 0.14	n.s.
Maximum tangent modulus [MPa]	31.3 ± 9.4	26.7 ± 7.1	<0.05	30.7 ± 7.3	32.1 ± 5.1	n.s.
Stiffness at $\sigma = 1$ MPa [10^3 N.m^{-1}]	37.32 ± 4.04	27.69 ± 9.03	<0.05	8.60 ± 2.62	10.01 ± 2.09	<0.05
Tangent modulus at $\sigma = 1$ MPa [MPa]	19.22 ± 2.08	12.63 ± 4.11	<0.05	6.28 ± 2.23	7.55 ± 1.69	<0.05
Thickness variance [mm]	2.06 (1.5—2.8)	1.82 (0.7-–2.8)	-	2.92 (2.5-–3.5)	3.02 (2.5-–3.8)	-

Table 5: Mean values of mechanical parameters of the measured samples with standard deviation values. The two final columns indicate p-value – the significance of differences between two groups; n.s. = not significant (two-tailed matched-pair t-test).

There were 18 samples of both the non-weight bearing zone and the defect zone group examined. Stiffness at $\sigma = 1$ MPa in the non-weight bearing zone group was

$(37.32 \pm 4.04).10^3$ N.m^{-1} while that for the defect zone group samples was substantially lower $(27.69 \pm 9.03).10^3$ N.m^{-1} ($p<0.05$, two-tailed matched-pair t-test). Significantly higher compliance of the defect zone cartilage proves, that it is a remarkable feature in distinguishing both the materials.

Stiffness of Type 3 chondrograft at $\sigma = 1$ MPa was $(253.34 \pm 74.16).10^3$ N.m^{-1} and tangent modulus at the same compressive stress (40.52 ± 11.86) MPa. These values are substantially higher than those of native cartilage. Still, visual comparison of the whole loading diagrams for non-damaged native cartilage and tissue-engineered chodrografts seeded with chodrocytes would reveal best resemblance for Type 3 chodrograft.

Besides studying complete compressive loading curves, it was also necessary to determine the compressive strength value. To obtain data for this ultimate value, the impact energy was increased step-by-step up to apparent tissue failure. In contrast to prevailingly linear elastic and brittle materials, the failure limit of living tissue is not so strongly defined. Fig. 22 illustrates the example of hyaline cartilage blunt impact tests. The force-displacement graph of the intact cartilage (c) shows the successive increase in hysteresis and residual strain (b, a). The area of the hysteresis loop increases at the expense of plastic deformation, resulting in large residual deformation and overall cartilage material deterioration. The material is then damaged to the extent that the deformation is non-reversible, even after a long recovery period. This failure criterion is similarly defined by Repo and Finlay, Jeffrey et al. and also Kerin et al. [21, 66, 98]. These authors suggested that a decrease in the graph's gradient and a widening of the hysteresis curve indicates region where irreversible damage and general failure occur. Nevertheless, the dynamic loading curves recorded by the instrumented impact testing more reliably identify the ultimate compressive strength.

The stress values were calculated for the appropriate cross-section area of the specimens (3.8–4.9 mm^2), with a cartilage-on-bone thickness of 0.8–3.8 mm. The compressive strengths were determined in the range of 5.46 MPa to 14.48 MPa. The corresponding strain values (ultimate strain) were identified in the range of $\varepsilon = 0.20$–0.74 for different materials. Along with these values, Tab. 5 shows also maximum tangent modulus near the failure point. It should be emphasized that the hyaline cartilage samples in this study were tested as circumferentially unconstrained. The specimens had a length to diameter ratio of nearly one, which is why bulging of the sidewalls was possible at loading.

Five samples for each of three types of grafts with cultivated chondrocytes were also examined for their mechanical properties. Fibrin chondrografts Type 1 were prepared in standardized procedure in the tissue bank. Grafts Type 2 and 3 were laboratory-prepared experimental samples, based on scaffolds manufactured solely for this testing purpose. In Type 2 and 3 grafts are thus possible slight variations in properties in

repeated production.

The behaviour of artificially cultured autologous chondrocytes formed into chondrografts is slightly different from native hyaline cartilage. As it is plotted in Fig. 23, their loading curves at the starting phase of compression are less steep (i.e. the tangent modulus is also small, material is less stiff) and the essential increase in loading force does not occur for Type 1 and 2 chondrograft until larger specimen deformation develops. This has occurred at 40–50 % compression of the specimen's thickness, even for relatively small impact energies. Nevertheless, even at such large compressions the material was not damaged and after 1–3 minutes regenerated its original capabilities. Ultimate compressive strength for these tissue-engineered materials can be assessed as 5–11 MPa (see Tab. 5). On the other hand, in Type 3 chondrograft the essential increase in slope of loading diagram curve appeared for strains of about 5 %. Under repeated testing shocks all three artificial materials behaved reversibly until the aforementioned values of compressive strengths were exceeded.

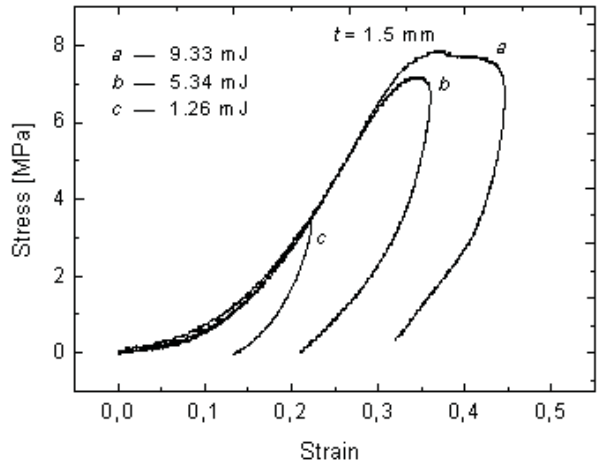

Figure 22: Occurence of hyaline cartilage specimen degradation after compressive strength overload.

3.4 Dissipated energy as an ultimate mechanical characteristic for cartilage condition assessment

3.4.1 Evaluation of dissipated energy from loading diagrams in blunt impact testing

Among mechanical quantities characterizing articular cartilage, those dealing with part of compressive energy lost within the tissue were so far neglected in cartilage research. Absolute and normalized dissipated energy as well as specific damping capacity were defined in section 2.2.4 (p. 26).

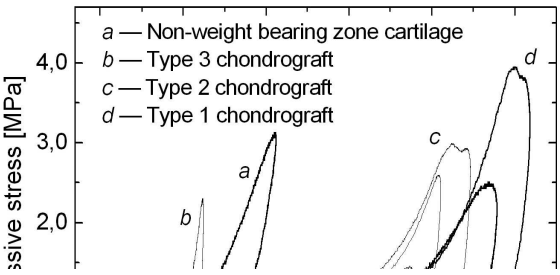

Figure 23: Typical compressive stress vs. strain dependence of human hyaline cartilage from non-weight-bearing zone and its comparison with chondrografts Type 3 (b), Type 2 (c) and Type 1 (d). Individual curves for samples c and d represent different impact energies.

Knowing the material loading curve hysteresis, energy dissipated during the impact can be evaluated. The ratio of dissipated energy ΔE to the overall energy of impact E_1, related to E_1 values can be plotted as it is shown in Fig. 24. For sake of figure clarity only measured values are depicted. As seen, the ratio of dissipated energy to the impact energy $\Delta E/E_1$ remains nearly constant after small initial decrease when related to E_1. In this interval the cartilage structure does not show symptoms of mechanical deterioration. Increase of the $\Delta E/E_1$ value at the higher impact energies indicates that the material suffered a certain degree of mechanical structural deterioration. The thicker the cartilage sample, the lesser are the differences in $\Delta E/E_1$ for different E_1 – thicker sample appears more durable. This factor should be taken into account when the mechanical damage limits need to be defined. The ratio $\Delta E/E_1$ is an intrinsic property of examined material as far as its internal structure maintains in certain condition. This value is usually denoted as specific damping capacity [99], eventually as energy absorption or loss ratio [100].

3.4.2 Correlation of retrieved mechanical characteristics with histological cartilage classification

Human knee cartilage samples of different quality were examined in pursuit of correlation of their mechanical, histological and macroscopic characteristics. Along with dissipated energy, tangent modulus and stiffness at 1 MPa stress were evaluated (as defined in section 2.2.4, p. 26). Maximum tangent modulus and stiffness at the upper extremity of loading curve were also evaluated. The samples were loaded with

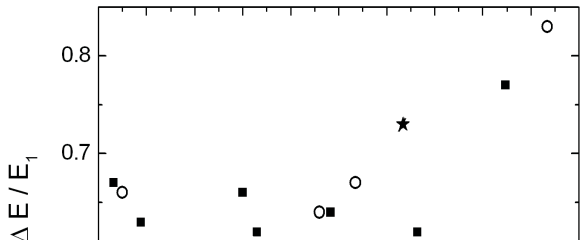

Figure 24: Specific damping capacity vs. stored compressive energy for three native cartilage specimens. Thickness l of individual samples denoted.

v_1=25 cm.s^{-1} initial impactor velocity (i.e. E_1 = 17 mJ).

Specific damping capacity and proportionally related absolute absorbed energy were the only mechanical characteristics revealing significant difference (ANOVA, $p<0.01$) between the groups 1—4 (Tab. 3, p. 36). Considering couples of groups (1 vs. 2, 2 vs. 3 etc.), significant difference was revealed between each two (T-test, $p<0.05$) except groups 1 and 2. No other mechanical characteristic did differ substantially between the groups.

Examples of loading diagrams for samples of different location and histologically assigned quality are given in Fig. 26.

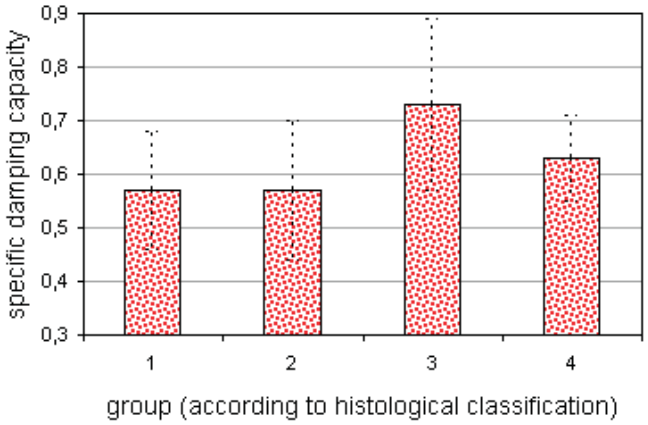

Figure 25: Specific damping capacity for individual groups of samples according to histological score, mean values with standard deviations shown.

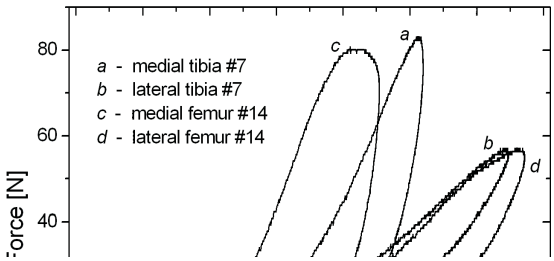

Figure 26: Examples of force-deformation loading diagrams for corresponding samples of different thickness and histological score. Medial (a, thickness 2.1 mm, total ICRS = 9, group 4) and lateral (b, 4.2 mm, ICRS = 14, group 2) tibial condyle of single joint; medial (c, 1.15 mm, ICRS = 12, group 3) and lateral (d, 3 mm, ICRS = 18, group 1) femoral condyle of single joint.

Regarding individual histological features separately, significant differences were found in specific damping capacity and proportionally related absolute absorbed energy as well as relative absorbed energy for features I, II and III. No other mechanical characteristics correlated significantly with the histological score (T-test, $p>0.05$). Mean values of specific damping capacity and tangential modulus at 1 MPa compressive stress for individual histological features are shown in Fig. 27 and Fig. 28.

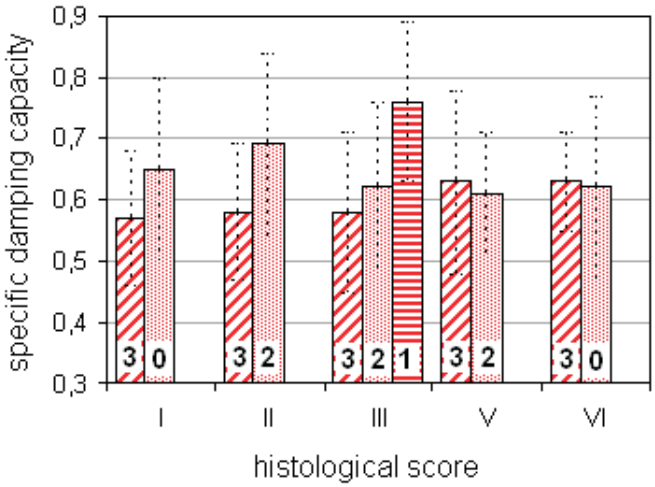

Figure 27: Specific damping capacity for achieved scores in individual features of histological classification, mean values with standard deviations shown. For feature no. 4 all samples scored the same, thus not provided.

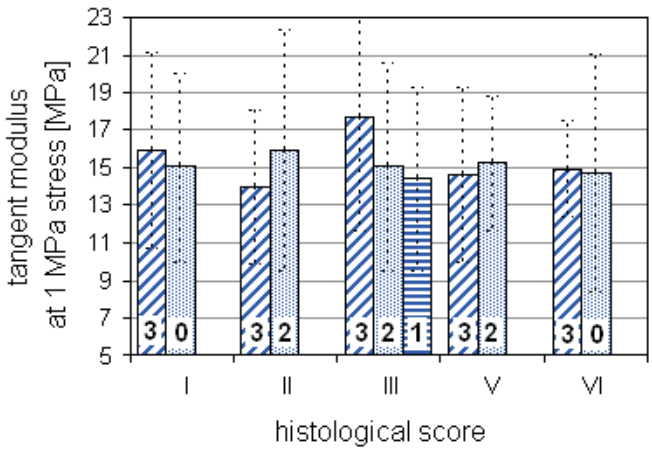

Figure 28: Tangential modulus of elasticity at 1 MPa normal stress for achieved scores in individual features of histological classification, mean values with standard deviations shown. For feature no. 4 all samples scored the same, thus not provided.

3.4.3 Correlation of retrieved mechanical characteristics with macroscopic cartilage classification

Significant correlation was again found between the macroscopic score value (Tab. 4, p. 36) and specific damping capacity and proportionally related absolute absorbed energy as well as relative absorbed energy (ANOVA, $p<0.01$). Neither stiffness nor elasticity modulus values followed the macroscopic ICRS classification.

Mean values of specific damping capacity increased between ICRS macroscopic grades 0 – 1 and 1 – 2 by 11.3 % and 18.6 % respectively. It implies that this material characteristic could serve for distinguishing between early stages of cartilage deterioration. Mean values of specific damping capacity for each of the ICRS macroscopic grades are shown in Fig. 29.

Medial condyles of both femur and tibia are in general more involved in load bearing, they are more stressed then the lateral ones. As the samples were harvested from the same spots in each examined knee, not regarding cartilage condition, more severe deterioration of medial condyles cartilage samples was expected (in accordance with e.g. [85]). This expectation was proved as shown in Fig. 30, relating the macroscopic evaluation to location of the samples within the knee joint. The same pattern is followed by values of specific damping capacity, as shown in Fig. 31. Even though it was previously reported that cartilage mechanical properties slightly vary with location within the knee joint [35], results shown in Fig. 30 prove that different locations also suffer different level of deterioration.

Though no correlation between cartilage samples thickness and total histological

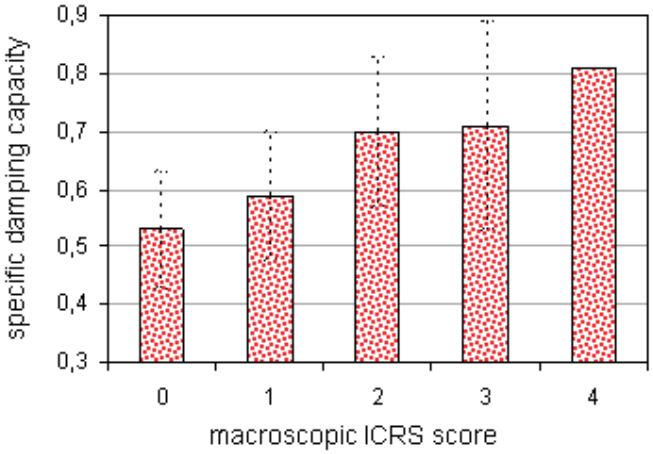

Figure 29: Specific damping capacity for individual classes according to ICRS macroscopic evaluation, mean values with standard deviations shown (in class 4 two samples only, thus no standard deviation shown.

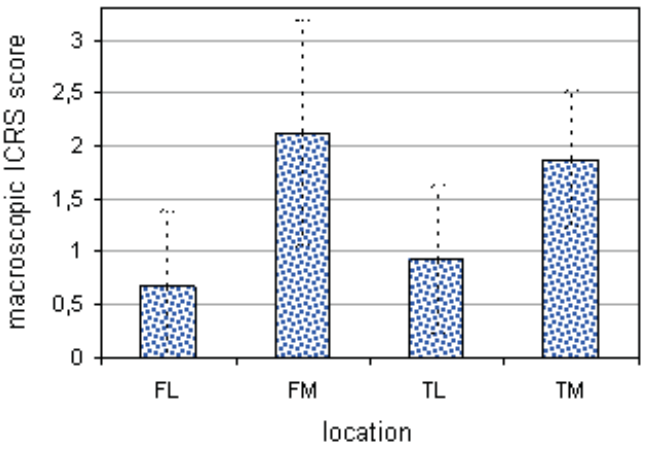

Figure 30: Macroscopic ICRS classification of cartilages according to location of sample harvesting, mean values with standard deviations shown (FL, FM — lateral and medial condyle of femur respectively; TL, TM – lateral and medial condyle of tibia respectively).

score was proved, cartilage thickness can be considered as a marker of cartilage condition (as it e.g. partially determines ICRS macroscopic classification). Strong relation was revealed between energy dispersed in unit volume – relative dissipated energy and cartilage thickness (Fig. 32; $p<0.001$; $R^2 = 0.69$ for linear correlation). On the other hand, no relation of specific damping capacity, absolute absorbed energy, stiffness or tangential modulus with cartilage thickness was found.

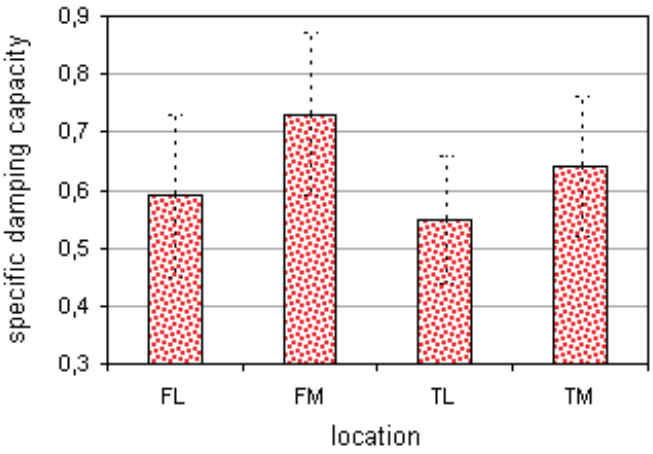

Figure 31: Specific damping capacity according to location of sample harvesting, mean values with standard deviations shown (FL, FM – lateral and medial condyle of femur respectively; TL, TM - lateral and medial condyle of tibia respectively).

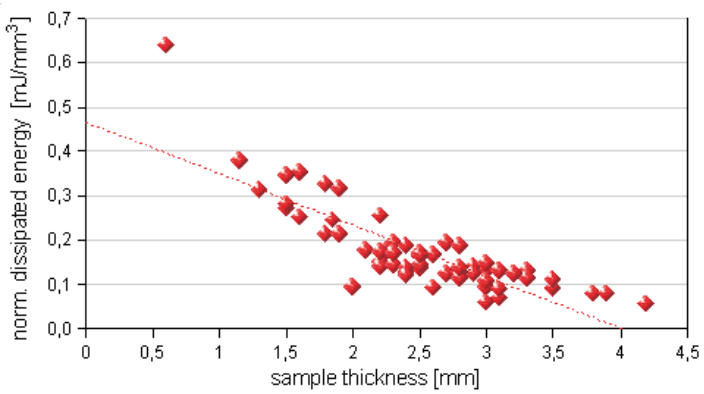

Figure 32: Relative dissipated energy (impact energy absorbed in unit volume of cartilage tissue) related to cartilage thickness, all measured values shown.

3.5 Quantitative features of loading diagrams in automatized characterization of cartilages in blunt impact testing

As a sequel of previous comparison of mechanical and histological performance of articular cartilage, a need for automatized objective evaluation of loading diagrams arose. Selected features of loading diagrams were calculated and their predictive capabilities examined.

More than 30 diagram features were checked and those with potential biomechanical meaning along with others showing signification when related to histological classification were treated further. For computation (and interpretation) reasons most of the features were computed separately for ascending and descending parts of the curve.

Parameters of Gaussian fit, length and slope of the curve, its overall and partial amplitudes and areas under the whole curve and its parts were found to be the most relevant ones for ascending and descending diagram part. The position of global maximum, area of hysteresis loop, tangent modulus and central moments (mean, standard deviation, skewness, kurtosis) were also evaluated for the whole diagram curves.

Results showing normal distribution and statistical significance of evaluated features for histological classification are displayed in Tab. 6 and 7. Features describing the whole loading/unloading process that were computed from the entire curve are shown in Tab. 8.

Evaluated feature	**Normal distribution**	**Significance**
A-up from GaussFitting	No	$p < 0.01$
S-up fromGaussFitting	No	$p < 0.01$
X_0-up fromGaussFitting	No	$p < 0.01$
Length of upwards curve	Yes	$p < 0.05$
Average slope upwards	No	-
Abs. amplitude in 1^{st} third of upwards curve	No	$p < 0.01$
Abs. amplitude in 2^{nd} third of upwards curve	Yes	$p < 0.01$
Amplitude ratio of amplitude in 1^{st} third of upwards curve to the whole upwards length	No	$p < 0.05$
Amplitude ratio of amplitude in 2^{nd} third of upwards curve to the whole upwards length	No	-
Area under the upwards curve	No	$p < 0.05$
Area under the 1^{st} third of upwards curve	No	$p < 0.01$
Area under the 2^{nd} third of upwards curve	No	$p < 0.05$

Table 6: Extracted features from the ascending (loading) force-compression curves. Their statistical significance is mentioned in respect to ICRS histological score. A, S and X_0 are parameters of non-centered non-normalized Gaussian fitting: $y(x) = A \exp\left(-((x - x_0)^2)/(2S^2)\right)$.

All extracted features were tested on normality of their distribution regarding each one of the five available histological scores (score IV is even for all samples). It is necessary to keep in mind the total numbers of samples in each class in Tab. 2 -– the results of normality tests are informative but statistically not significant. Kruskal-Wallis test was performed on all features. Significances in Tabs. 6, 7 and 8 represent the best significance of the feature obtained over all the five possible scoring subsets. The features extracted are not necessarily significant for all histological scores, but in most of the features are significant for at least one score.

Evaluated feature	Normal distribution	Significance
A-down from GaussFitting	No	-
S-down from GaussFitting	No	$p < 0.01$
X_0-down from GaussFitting	Yes	$p < 0.05$
Length of downwards curve	Yes	$p < 0.01$
Average slope downwards	No	$p < 0.01$
Abs. amplitude in 1st third of downwards curve	No	$p < 0.01$
Abs. amplitude in 2nd third of downwards curve	No	-
Amplitude ratio of amplitude in 1st third of downwards curve to the whole downwards length	No	-
Amplitude ratio of amplitude in 2nd third of upwards curve to the whole downwards length	No	$p < 0.01$
Area under the downwards curve	Yes	$p < 0.05$
Area under the 1st third of downwards curve	No	-
Area under the 2nd third of downwards curve	Yes	$p < 0.05$

Table 7: Extracted features from the descending (unloading) force-compression curves. Their statistical significance is mentioned in respect to ICRS histological score. A, S and X_0 are parameters of non-centered non-normalized Gaussian fitting: $y(x) = A \exp\left(-((x - x_0)^2)/(2S^2)\right)$.

Evaluated feature	Normal distribution	Significance
Amplitude of curve maxima	Yes	$p < 0.01$
Position of amplitude maxima	Yes	$p < 0.05$
Position of max. amplitude (force) relative to max. curve position (compression)	No	$p < 0.05$
Dissipated energy	No	$p < 0.05$
Tangent modulus at 1 MPa stress	No	$p < 0.01$
Mean	No	$p < 0.01$
Standard deviation	No	$p < 0.01$
Skewness	No	-
Kurtosis	No	-

Table 8: Extracted features based on the whole force-compression loading curves. Their statistical significance is mentioned in respect to ICRS histological score.

The basic principle of induction of decision trees such as the one used in this experiment – C4.5 implementation in the Weka [101] environment called J48 – is to count entropy of attributes, then to create node from attribute with the maximal entropy. In the final step the algorithm removes all branches that do not improve the accuracy of the tree [93, 101]. Example of the rules in decision tree about the final score of the sample can be seen in Fig. 33.

```
if A_up_GaussFitting  <= 52
    if Area_under_the_1/3of_upwards_curve <= 48100
        if    absl_3rdFdo <= 6.1,
            sampleClass = Normal (4.0)
        else sampleClass = Abnormal (2.0) end
    else sampleClass = Normal (31.0) end
else
    if Energy_Fup_ <= 1624129
        if  gauss_up_S_ <= 319
            sampleClass = Abnormal (5.0)
        else sampleClass = Normal (3.0/1.0) end
    else sampleClass = Normal (3.0); end
end
```

Figure 33: Sample of derived decision tree for classification into two classes for score VI.

3.6 Impact testing method in tensile examination of ligaments and tendons

Same measurement principles as introduced for impact compressive testing can be exploited in impact tensile testing experiments. Apparatus for dynamic tensile testing was constructed and experiments to assess mechanical properties of human anterior cruciate ligament and grafts for its potential transplantation conducted.

For tensile response characterization, the elastic modulus related directly to stiffness can be approximated as the gradient of the stress-strain loading curve. At the beginning of loading, the loading force increases and the stiffness increases as well. Under natural conditions the tendon's tension must not exceed a nominal linear value if irreversible damage is to be avoided. Consequently, ultimate tensile strength is defined as the maximum resistance to tensile loading stress. Stiffness is defined in $N.mm^{-1}$ as the resistance to elongation at the linear region. Unlike the stress vs. strain dependence and the elasticity modulus, both the tensile strength and stiffness values are proportional to the cross-sectional area. The latter parameter can thus vary for each of the tendon specimens. Figs. 34 and 35 show the typical dynamic loading diagrams of tendon specimens.

All the specimens were measured for their response to the dynamic tensile load. Besides the absolute loading force values, the ultimate tensile strength values were also evaluated and calculated for the corresponding section area of the specimen. The

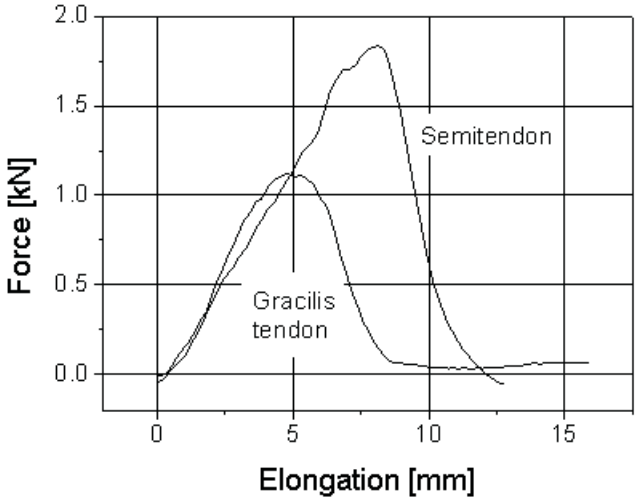

Figure 34: Dynamic loading force vs. elongation for one of the specimens of gracilis tendon and semitendinosus.

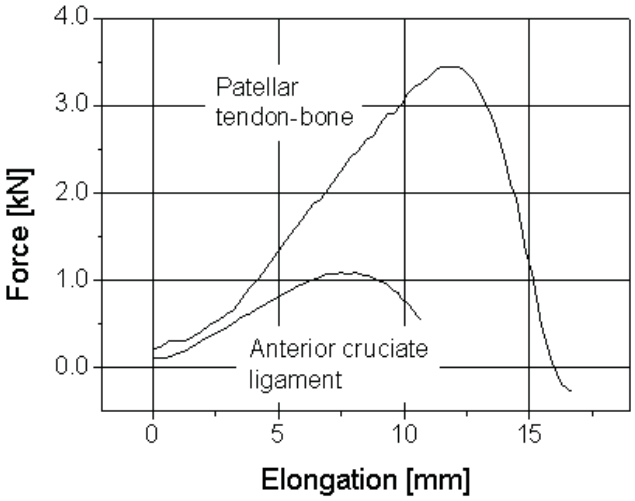

Figure 35: Dynamic loading force vs. elongation for the specimens of patellar tendon-bone and anterior cruciate ligament.

tensioned strands of the original ACL showed a maximum average load of 1246 ± 243 N in the section area of about 30 mm² (ult. strength 41.3 MPa), strands of Bone-Patellar Tendon-Bone (BPTB) grafts showed values of 3855 ± 550 N in the section area of 80 mm² (ult. strength 40.6 MPa), hamstring tendons gracilis showed 925 ± 127 N in the area of 10 mm² (ult. strength 95.1 MPa) and semitendinosus yielded a result of 2050 ± 159 N in the area of 20 mm² (ult. strength 88.7 MPa). The elongation limit – the maximum strain before real disruption – was about 20 % for all the specimens.

Sample	**No. of strands**	**Max. load [N]**	**Stiffness [N.mm^{-1}]**	**Ult. strength [MPa]**
ACL	single strand	1246±243	182±37	41.3±8.1
BPTB	single strand	3855±550	364±54	40.6±7.1
gracilis	single strand	925±127	354±49	95.1±13.1
	double strand	2573±496	432±83	90.3±17.4
semitendinosus	single strand	2050±159	224±20	88.7±7.8
	double strand	3395±592	487±85	82.6±14.4
gracilis - semitendinosus	quadruple strand	4546±1500	490±161	70.6±23.3

Table 9: The ultimate loads, stiffness and maximum stresses of measured specimens.

According to the results, all of the tested grafts showed higher stiffness and durability then the cruciate ligament. Tab. 9 summarizes the measured values of maximum loading force, stiffness in the linear region and also the ultimate tensile strength for different types of tendons.

Besides the single strands, the ultimate values of doubled and quadrupled grafts are also given in the Tab. 9. As can be seen, their tension per section area approaches the values for single strands. The non-significant decrease in maximum values is evidently caused by good but not ideal fixation of the elements, where a small amount of pull-out tends to reduce these values. We assume that it is the only factor causing this effect.

4 Discussion

4.1 Blunt impact testing is a consistent method for retrieval of cartilage tissue characteristics

As a commencement of cartilage mechanics investigation using novel setup, measurements were taken to reveal reliability of the method and repeatability of measurements. Differences in examined pig knee cartilage samples were most probably of diverse origin, ranging from individual anatomical and physiological condition of animals over different tissue location from which the sample has been collected to possible inaccuracy of sample preparation and its orientation in measurement process. However, the major scatter may have occurred due to sample shape, positioning and dimensions determination. Presented extent of statistical variance, which did not exceed 25 % (Fig. 14, p. 39), can be regarded as fully satisfactory for considered purpose. In following experiments we have tried to avoid and suppress the listed sources of inaccuracy as much as practically feasible.

For evaluation of mechanical response of tested materials the standard, well defined quantities were used. Entire loading diagram curves were acquired in introduced blunt impact testing. They enabled also evaluation of further important characteristics, such as dissipated energy and values of ultimate loading (Fig. 15, p. 39).

For the testing with circumferentially unconstrained and unconfined specimens there is a characteristic feature of interstitial fluid escape, as was noted by several authors [21,31,66,90]. Under these conditions in quasi-static compression, the unloading part of the loading curve sharply falls. Anelastic recovery or even permanent strain meaning irreversible plastic deformation takes place in this situation. The short-time irreversibility of the process is caused by a squeeze of the fluid from the material elastic matrix, presuming extracellular matrix was not damaged.

At higher strain-rates cartilage appears stiffer – slope of the loading diagram is thus higher and reaction is more elastic – lesser residual strains and lower energy loss are observed, as it is typical for viscoelastic materials (Fig. 16, p. 39). The dynamic test curve is always shifted compared to that of static one. It has to be noted that the nonlinear shape of each loading curve results predominantly from large strains of unconfined compression, as the interstitial fluid flow within the tissue is sufficient for its escape from the material structure at low loading rate. The poroelasticity of tissue, which is due to viscous fluid flow inside the material, is reflected mainly in the hysteresis curve shift with respect to strain scale. Hysteresis loop of the quasi-static test curve is then wider and, consequently, its area is larger than that of the dynamic test curve. The loop gets even narrower as the strain rate increases. The area under the shock

test curve tends to be smaller, as was proved by impact experiments (see Fig. 16). From this it emerges that energy losses in articular cartilage tissue impact loading are smaller in comparison to the low loading rates. It implies that the material reacts to impact loads in a more elastic manner and its compression deformation changes are to large extent reversible. The steeper course of loading diagrams at higher loading rates is in accordance with documented increase of dynamic compressive modulus at higher impact energies and loading rates in impact testing [23] as well as higher dynamic compressive modulus values at higher loading frequencies [40].

The brief preview of cartilage mechanical response modeling (section 2.1, p. 21) shows that cartilage as a viscoelastic material could be described by two-parametric analytical model in a satisfying manner. The model (Eq. (1), p. 21) regards the acting forces and suits macroscopic characterization of the material. General approach in modeling of articular cartilage properties is based on function of cartilage components. Firstly bi-phasic exponential model was introduced, considering solid and liquid cartilage environment [65, 102–104]. Later tri-phasic model dominates, taking into account as well fixed charge of glycoproteins [27, 105].

4.2 Loading diagram achieved in blunt impact testing serves as an appropriate tool for qualitative comparison of different materials

Results of introductory experiments served solely comparative purposes. Qualitative evaluation of loading diagrams without necessarily evaluating mechanical quantities can be valuable in mechanical behaviour assessment. This comparative approach was used to characterize several different tissue engineered scaffolds. Scaffolds presented in Fig. 18 (p. 41) and Fig. 19 were according to revealed mechanical response found to be suitable as eventual cartilage tissue substitutes. Both knitted Chirlac scaffold and collagen enriched fibrin scaffold were thus subjected to further *in vitro* and *in vivo* experiments examining their applicability in autologous chondrocytes implantation [94, 95].

Scaffolds containing macromolecular components, expected to improve their biological and mechanical characteristics, were finally tested in a rabbit model [95]. As presumed [106] and experimentally confirmed, collagen content in fibrin gel remarkably increased its stiffness. Hyaluronic acid content appeared to be mechanically relevant as well, as the material stiffness did not strictly follow the amount of collagen incorporated. Moreover, the scaffold composition did seem to create a suitable environment for cell seeding and adhesion. Even the healing process was accelerated when using these scaffolds [95]. It was concluded, that the scaffold is able to induce early cartilage

regeneration, being a promising material for cartilage repair.

Comprehensive mechanical characteristic of examined material is available in complete loading diagram forming a hysteresis loop. Several quantities are used for evaluation of these characteristics in practice, but they can hardly deliver the entire information. Still, these quantities are necessary as visual consideration and verbal description is not applicable in more extensive studies. Examples of loading diagrams of intact and impaired human articular cartilage were presented in Fig. 21 (p. 43). Healthy cartilage response consists of nearly linear part characterizing elastic matrix, followed by steep non-linear part caused mainly by viscoelastic properties of extracellular matrix and interstitial fluid. In damaged cartilage diagram changes often occur in favor of linearity (damaged porous structure, lack of fluid content), as seen in Fig. 20 (p. 42), or when an almost immediate deformation to substantial extent occurs, followed by sudden diagram course change to viscous curve (loss of matrix elasticity, increased porosity and water content) – Fig. 26 (p. 49). Similar drawbacks and limitations are typical in designed artificial tissue materials.

4.3 Mechanical parameters of native and tissue engineered cartilage revealed in blunt impact testing

The tissue-engineered cartilage used nowadays as hyaline-like cartilage for autologous chondrocyte implantation in reconstructive surgery must be anatomically suitable and biocompatible, corresponding to the mechanical properties of human cartilage. The suitability of substitute materials depends on the requirements of the original cartilage type and on its standard mechanical function. For this purpose, standard characteristics of human articular cartilage are being examined, with a prospect to explain properties of the extracellular matrix [31, 107, 108].

4.3.1 General findings on cartilage mechanical properties

Measurement settings have been chosen according to available knowledge about dynamics of physiological loading of articular cartilages. Values were specified in section 1.3 (p. 9) and 2.2.3 (p. 26). Employment of physiological strain rates along with compressive stresses up to ultimate values make this study rather unique.

The known experimental studies on impact testing of articular cartilage have been basically oriented to determine compressive strength (e.g. [21, 23, 24]). The described approach of instrumented impact testing enabled detailed quantitative investigation of the acting dynamic forces and corresponding deformation responses, within a large range of loading rates, from the low to rapid impact characteristics.

Owing to the nature of the cartilage tissue, it is possible to study the continual rapid increase of stiffness activated by the poroelastic fluid flow effect [107,109]. Under dynamic loading, the hydraulic permeability of the solid matrix of the intact hyaline cartilage effectively regulates the material's compression. The cartilage poroelastic nature was confirmed also by the shape of the loading curves. The initial parts of ascending dependencies at different impact velocities coincide to a large extent but at higher stresses the tissue appears to be stiffer for higher loading rates due to increased pressurization and resistance to fluid flow (Fig. 21, p. 43 and Fig. 23, p. 47).

We have also empirically experienced that the hyaline cartilage can regenerate its initial state of mechanical properties within a time interval of several tens of seconds. This reversible process is repeated until the compression stress reaches a defined ultimate level, when irreversible defects are initiated. As the process of mechanical damaging is gradual, the hyaline cartilage progressively loses its capability to resist large deformations (see Fig. 22, p. 46). Destructive processes thus do not appear suddenly – this observation seems to have a crucial meaning for general cartilage failure prevention and the rehabilitation process of patients.

Plotting the characteristics of materials from both the non-weight-bearing and the defect zones in a single graph clearly indicates measurable differences in stiffness across a range of impact energies (velocities) in individual samples. Furthermore, at the same impact energy damaged tissue shows larger deformations (Fig. 21, p. 43), as it is obviously more stigmatized by structural deterioration. This finding is in coincidence with the observation of other authors [42, 43, 98]. With increasing impact energy also the area of hysteresis loop has increased, meaning a larger absolute value of impact energy was absorbed. Our findings coincide with the statements of Kerin et al. [66] where also the enlargement of the hysteresis loop area was observed at higher levels of loading at nearly ultimate values. Comparison of energy absorbed within intact and damaged cartilage were subject to further experiments.

The decrease in poroelastic capabilities resulting from disease-related degradation creates the risk of increased compression deformation at heavier shocks, with subsequent serious consequences in structural damage. This phenomenon is apparently also intensified by concomitant reduction of cartilage thickness.

4.3.2 Revealed mechanical characteristics of native articular cartilage

It has been shown that the measurements are not unacceptably affected by the determination of precise size and shape irregularities of the samples, perhaps with minor exception in correctly defining cartilage-subchondral bone interfaces. Evaluating eighteen cartilage-on-bone samples, with multiple loadings on each of them, has gained

quite extensive set of results. It appears sufficient for their mutual comparison and for determination of their relationships.

Our findings of structural integrity limits in the stress range of 5.46–14.48 MPa are smaller than those of the older measurements by Repo and Finlay [21], where the critical limit was determined by drop-tower testing as about 25 MPa at strain rates of 500 s^{-1} and 1000 s^{-1} (corresponding to maximum 25 % strain). Moreover, in other experiments measured as static loadings on bovine articular cartilages a nominal applied stress was determined in the range of 14–59 MPa (mean 35.7 MPa) for structural failure [66]. Ultimate values for mean peak stress and corresponding strain in bovine articular cartilage in impact testing were found to be 16.7 MPa to 27.4 MPa and 0.44 to 0.68 respectively [24]. Given range corresponds to different impact energies used. These values are almost twofold of the results we have achieved with human articular cartilage. The difference might have appeared due to different cartilage nature, different sample mounting as well as different measurement procedure. Analogous experiment on bovine cartilage [23] revealed maximum dynamic modulus of 86 MPa to 237 MPa depending on impact energy and loading rate. We report here maximum tangent modulus of approximately 30 MPa – difference may be again attributed to the same reasons as listed above. Smaller ultimate compressive strength values of our tested samples can be partially explained by the fact that all the tests performed were realized as circumferentially unconstrained loadings on relatively long cylindrical samples where bulging of sidewalls was present. The most important reason for mentioned partial discrepancies are substantially lower strain rates then those used in cited impact loading studies. They were used here in order to simulate physiological loading.

Values of compressive modulus in uniaxial confined compression and indentation configurations have been reported in range 2–10 MPa [110–113], compressive modulus was found to decrease with progressing damage in animal models [114]. Human knee cartilage was reported to possess compressive modulus ranging from 1 MPa to 19.5 MPa according to sample harvesting location (femur, tibia, patella) [35]. Our findings fall well within this interval, though mainly to its upper portion, which is contributed to impact loading rates used in our study.

When Young's modulus of chondocytes was examined in non-osteoarthritic cartilage and cartilage of terminal osteoarthritis stage no significant differences were found [115], thus mechanical changes in affected tissue should be contributed to modified properties of extracellular matrix.

4.3.3 Revealed mechanical characteristics of tissue-engineered cartilage

A variety of natural and artificial scaffold materials has been designed for chondrocyte growth and differentiation up to date. The core processes for the treatment using chondrocytes are *in vitro* cultivation of cells and combination of chondrocytes with scaffold material to produce tissue-engineered cartilage. However, the monolayer growth of chondrocytes often causes dedifferentiation, resulting in immature cartilage. For this reason it is important to evaluate the status of the chondrocyte cells differentiation, which in turn indicates the quality of the engineered cartilage [66]. In this study, the presence of viable chondrocytes was confirmed in both Type 1 and Type 2 grafts, in Type 2 with a higher amount of living chondrocyte-type cells. Suitability of Type 3 chondrograft was proved previously [95]. On contrary, the presence of chondrocytes in the native hyaline cartilage depends on the severity of deterioration in examined area.

Examined chondrorafts revealed 26.8 % and 23 %, i.e. approximately 1/4 of healthy cartilage stiffness respectively for chondrografts Type 1 and Type 2. Type 3 chondrograft did exhibit 6.7 times higher stiffness than the non-damaged cartilage at normal compressive stress of 1 MPa. The results gathered for tangent modulus at 1 MPa stress were: 39 % for Type 1; 32.7 % for Type 2 and 211 % for Type 3 chondrograft when compared to non-weight bearing zone cartilage. Regarding solely these values, fibrin scaffolds appear more compliant, while the collagen and hyaluronate enriched one stiffer than native cartilage. Substantial difference is that in very initial phase of loading (up to 5 % strain) Type 3 chondrograft is more compliant than the cartilage tissue, while afterwards its stiffness arises steeply, resulting in characteristics of loading diagram slope being multiples of those describing native tissue. This status was intended as it was expected according to previous tests within rabbit model studies (results presented in section 3.2, p. 40).

Fibrin scaffolds have been already approved for human ACI surgeries and provide very satisfying results (e.g. [16]). In animal experiments, as already mentioned, the enriched Type 3 chondrografts provided better cartilage regeneration then was previously found with the fibrin scaffolds [95]. From the mechanical point of view, chondrograft Type 2 differs significantly from Type 1 in favour of native cartilage properties. Despite this fact, when compared to mechanical response of native cartilage both fibrin scaffolds exhibit comparably divergent properties (Fig. 23, p. 47). Even though the evaluated quantities prove the Type 3 chondrograft to be several times stiffer than native tissue at 1 MPa compressive stress, loading diagrams (Fig. 19, p. 42) document that overall mechanical response of Type 3 chondrograft resembles the native tissue better then the fibrin graft.

Modifications in fibrin scaffolds production thus seem to bring a real chance in en-

hancing chondrograft mechanical properties. Alternative approaches aiming to solidify the scaffold though may turn up to be much more efficient – as demonstrated by slight but well founded change in chemical composition. Collagen enriched scaffold has been again proved to be a promising material for chondrocytes transplantation.

To summarize presented information relevant for rehabilitation of patients who underwent articular cartilage transplantation, there are two facts worth empathizing: (i) Even the lowest possible ultimate values for cartilage loading should be avoided. That should ensure protection of regenerating cartilage from irreversible damage. According to our measurements compressive stress thus should not exceed 5 MPa. This would mean e.g. for knee joint loading force approximately up to 2500 N. According to this simple reflection, implanted chondrograft should withstand loads typical for normal gait (section 1.3, p. 9). (ii) At higher strain-rates, cartilages as well as chondrografts react in more elastic manner. Lower residual strain is present, less energy is dissipated and the tissue is thus more likely to fully restore its mechanical capacity. Therefore in rehabilitation faster joint loading should be preferred to the slower one.

4.4 Dissipated energy is an ultimate mechanical characteristic for cartilage condition assessment

Dissipated energy or so-called energy loss, understood here as part of the impact mechanical energy transformed to different energy form, is along with elastic moduli and stiffness an important quantity characterizing mechanical properties of tested material. When there is no dissipated energy, we deal with ideal elastic material, while when all the energy appears to dissipate no real elasticity is observed. The extent of mechanical energy lost by dissipation also depends on strain rates and acting forces (as seen in Fig. 16, p. 39). Dissipated energy thus appears crucial in cartilage biomechanics evaluation.

4.4.1 Correlation of retrieved mechanical characteristics with histological cartilage classification

Harvested cartilage samples were sorted into four groups according to severity of their histologically revealed disruption (Tab. 3, p. 36). This was meant to simplify the complex histological categorization (Tab. 2) and eventually find correlation between mechanical features and actual level of tissue damage.

None of the differences between individual groups in listed mechanical features can be considered substantial. Even the difference in specific damping capacity is ambiguous, as can be seen in Fig. 25 (p. 48). This might be caused by the fact, that though decreasing value of each histological feature score reports on more serious

cartilage damage, from mechanical point of view these degenerative changes do not necessarily have to have the same consequences. Mineralization (feature VI) could be expected to increase affected cartilage stiffness. On the other hand, disorganization in chondrocytes distribution (feature III) would be expected to hamper the tissue integrity and thus its stiffness. Fibrocartilage was previously reported to possess lower dynamic modulus than hyaline cartilage [40], therefore fibrotization of articular cartiage (feature II) should as well decrease its stiffness. Effect of uneven cartilage surface (feature I) on measured stiffness would be quite unpredictable. Also effects of individual histologically revealed impairments on amount of impact energy dispersed in the sample is beyond simple rational assessment. Evaluation of summation score thus does not appear to be a relevant cartilage characteristic, which agrees with ICRS recommendations [116].

When comparing biomechanical properties of samples regarding individual evaluated histological features, only the values characterizing dissipated energy were found to be in significant relation. This was proved for histological features I–III, i.e. surface quality, degree of fibrotization and cell distribution. The fact that features V and VI did not show significant correlation might be partially caused by the uneven distribution of samples for the individual score values (43:8). Though stiffness and modulus of elasticity follow the expected trend (Fig. 28, p. 50), this cannot be considered significant due to high variance of obtained values. Generally, having only 2 subgroups with continuous qualitative transition for each histological score makes it difficult to show a statistical significance of their discrepancies.

Complementary samples from single joint, presenting different stages of cartilage damage, exhibit obviously different mechanical properties in each of evaluated characteristics (examples in Fig. 26, p. 49). General interdependence in terms of stiffness and tangential modulus was not observed in spite of the expectations. Along with previously mentioned causes, an important reason for not revealing this correlation were different locations of cartilage sample harvesting. In our experiment four different locations within the femoral and tibial articular cartilage were involved. It was previously reported, that compressive modulus values substantially vary according to knee joint topography [35, 117, 118].

According to so far reported studies, moderate correlation was found between the Young's modulus and histological Mankin score [85], compressive modulus decrease with increasing severity of degradation assessed using histological and histochemical grading was introduced [112], correlation in shear modulus and modified histological Mankin score using dynamic indentation was as well proved [69] etc. Our results as well confirmed relation of mechanical properties of articular cartilage to its histologically approved condition.

4.4.2 Correlation of retrieved mechanical characteristics with macroscopic cartilage classification

Macroscopic cartilage quality evaluation according to ICRS correlates with histological examinations, and is thus believed to be a reliable method for classification of degenerated cartilage [85]. We have also confirmed, that biomechanical cartilage parameters follow similar pattern using either macroscopic or histological cartilage quality assessment (Fig. 27 on p. 49, Fig. 29 on p. 51).

In all presented results, quantities characterizing dissipated energy revealed correlation to the cartilage condition. Decreased cartilage quality, according to either histological or macroscopic evaluation, has always meant an increase in absolute and relative dissipated energy as well as specific damping capacity value. This was confirmed also by relating these quantities to location of cartilage *in situ*. As expected and documented by macroscopic ICRS score values, cartilage of medial condyles generally suffers more severe deterioration (Fig. 30 on p. 51). Equivalent evaluation can be thus given in terms of dissipated energy – namely e.g. specific damping capacity.

Kleemann et. al [85] reported stiffness (Young's modulus) reduction with cartilage degeneration – increasing macroscopic ICRS score and histological appearance according to Mankin [82]. They predict cartilage stiffness loss of about 25 % for each ICRS macroscopic grade. Biomechanical characteristics were acquired in quasi-static setup. Our results in dynamic impact testing have not proved this relation.

No correlation between cartilage thickness and its stiffness or tangential modulus was proved in our study, which is in accordance with Bae et al. [42]. Shepherd et al. [119] report of compressive moduli correlating with cartilage thickness, but the condition of cartilage is not mentioned – probably presuming unimpaired tissue. Shepherd points out only slight correlation of lower limb cartilage thickness and physiognomical parameters of the donor. Here we presume that lower cartilage thickness is at least partially caused by its deterioration. As stiffness and elasticity modulus are determined by material composition and its condition rather then by its amount, we find our results reasonable.

Generally, difficulties in distinguishing between healthy articular cartilage and the one suffering initial stages of degradation is reported [85]. Young et al. [69] have evaluated dynamic mechanical properties (shear modulus and phase lag) of human tibial cartilage using specially designed indentor. They have involved only cartilages of 0 or 1 ICRS macroscopic score and related results to histological findings, concluding that mechanical analysis is sensitive enough to help in staging cartilage disease. Worth mentioning is that evaluated mechanical quantities are proportionally related to dissipated energy. Evaluation of indentation stiffness lead to similar conclusions [42, 46]. Our

results show differences of more than 10 % in values of specific damping capacity between groups scoring 0, 1 and 2 in ICRS macroscopic classification. Dissipated energy might thus, after more thorough survey, serve as an indicator for early osteoarthritis recognition.

Verteramo et al. [24] have evaluated mechanical properties of bovine articular cartilage under impact loading conditions resembling high joint load up to impact trauma. Presented mean values of energy absorbed per unit volume at different loading energies ranged from 3 to 13 mJ.mm^3 which meant approximately 0.6 % of the applied impact energy. Different study dealing again with bovine cartilages in similar experimental setup revealed absorbed energies per unit volume to be approximately 2.5 % and 8 % for different loading rates [23]. In our experiments we have used lower impact energies still with comparable percentual energy absorption in unit volume. According to cartilage condition, revealed energy loss per mm^3 varied from 0.3 % to 2.2 %.

Dissipated energy has not been yet, according to our knowledge, been taken for a representative feature of cartilage status. Though, it has been reported that increasing mechanical damage of articular cartilage leads to greater energy absorption [23]. In drop-tower dynamic impact testing [23], no correlation between energy of deformation per unit volume (relative dissipated energy) and cartilage thickness was found for bovine forelimb articular cartilages. In mentioned study, quality of cartilage was not assessed, only mechanical properties at different conditions were evaluated — presumably the cartilages were considered intact prior to testing. Furthermore, much higher impact energies and strain rates were used. These might be the reasons for substantial anticipation to our results, which have shown significant correlation of relative dissipated energy and cartilage thickness. Once we accept amount of dissipated energy as a quantifier of cartilage condition, this relation proves that the cartilage thickness describes cartilage quality as well – the thiner the cartilage, the more "unhealthy" it is. In partial contradiction, Broom et al. [120] conclude, that neither compliance of on-bone articular cartilage nor thickness measurements necessarily constitute sensitive indicators of biomechanical health of cartilage.

Being conscious of high variance of acquired data, we contribute this fact mainly to not absolutely exact description of samples – cartilage-bone interface not ideally perpendicular to the acting force direction, uneven cartilage surface, problematic classification of border cases in histological or macroscopic evaluation etc. These limitations can hardly be avoided, when examining native tissue samples without any customization for measurement and data processing needs. Substantial variance of acquired results is thus quite common in similar studies [29, 69, 85].

4.4.3 General considerations on dissipated energy as a marker for cartilage quality assessment

As already explained, elastic and tensile cartilage properties are determined mainly by solid extracellular matrix. Cartilage stiffness depends on both solid and fluid component. Dissipation of energy is attributed to interactions between components of solid matrix, which are expressed in shear modulus, and to dynamics of interstitial fluid [121]. Elastic moduli and cartilage stiffness decrease have been already quite frequently reported to accompany degenerative processes in cartilage tissue (e.g. [29, 69, 85, 115]). Dissipated energy has been so far a neglected feature. No studies were found reporting dissipated energy as a cartilage quality marker, though its evaluation in dynamic tests was pioneered [23] and its employment for comparative studies proposed [40]. In different fields of biomedical research is this approach also quite rare (e.g. [100, 122]). According to the results of our study, dissipated energy appears to be remarkably more significant quantifier of alterations in cartilage condition than above mentioned quantities.

Structural changes causing alteration of mechanical properties in degraded articular cartilage

Mechanical changes of cartilage tissue during the degeneration process are caused by changes in composition and integrity of cartilage. It has been reported, that the structural changes (loss of extra cellular matrix integrity) are superior to alterations in composition [46, 85]. Only minor changes in composition between native and degenerated cartilage are apparent while major ones in structure can be described. Macroscopic consequences of integrity loss are superficial irregularities and fissures in the mild stage and deep clefts, matrix disorganization and extended erosion in advanced stages of osteoarthritis. Composition changes affecting cartilage mechanics are mainly related to changes in water content, collagen integrity and amount of glycosaminoglycans present. Mechanical properties of chondrocytes remain unchanged in degeneration [123].

Along with structural changes, progressive cartilage thinning is reported with higher degree of its deterioration [124, 125]. These changes are closely related to changes in subchondral bone structure and thickness.

Changes in mechanical environment of chondrocytes have been shown to affect metabolic activity of cartilage and thus maintenance of the tissue. Some mechanical events may even alter activities of chondrocytes in the manner causing cartilage degeneration [2].

It is assumed, that collagen network fatigue is a primary factor in progressive cartilage damage and arthritis [126]. In osteoarthritis, excessive type II collagen degradation first appears close to articular surface [2], leading to cartilage fibrilation and weaken-

ing of collagen network. Local loss of proteoglycans follows this process. Damage then extends down to the matrix deeper zones. (On the other hand, in rheumatoid arthritis collagen degradation appears to start in the deep zone of cartilage.) Both PG content and size decrease with increasing severity of osteoarthritis [2]. If collagen network is damaged in some way, as usually occurs during osteoarthritis, the tensile modulus decreases dramatically [2]. Typically, osteoarthritic tissue also shows an increase in water content and mentioned decrease in content of PGs [112, 127]. Subsequently, not only collagen network but also collagen-proteoglycan matrix fails during osteoarthritis. Matrix porosity increases, thus its permeability increases as well and density of fixed charge decreases, resulting in decreasing compressive modulus and cartilage stiffness. Consequently interstitial fluid flow velocities increase and its pressurization decreases in altered cartilage [128, 129].

Mechanisms of energy dissipation in altered articular cartilage

Extracellular matrix of healthy cartilage is obviously more organized and dense than the one of altered tissue. Still, main mechanism of energy dissipation in healthy cartilage is believed to be friction between fluid component and porous structure of extracellular matrix [2]. Amount of dissipated energy is proportional to flow rate of interstitial fluid within the cartilage structure, as energy in general is defined as pressure times volume product. Considering real Newtonian fluid, resistance to flow is indirectly proportional to fourth power of tube diameter according to Poiseuille's law. Even though not talking about a tube stream geometry, increase in cartilage porosity is an analogous situation. If flow rate under certain pressure gradient increases approximately with fourth power of pores size, so does the lost energy. Therefore dissipated energy should be even in theory expected to be the most sensitive marker of cartilage condition. This fact was approved by the presented experimental results. These results have shown substantial increase in dissipated energy even when comparing intact cartilage to ICRS macroscopic grade 1 cartilage, which were so far considered to be hardly distinguishable in practice.

It ought to be reminded again, that the measurements were taken in unconfined compression though substantially higher interstitial fluid leakage was possible compared to physiological circumstances.

An opinion can be found, that cartilage can be considered elastic rather then viscoelastic [130]. This is based on referenced results assuming that rapid loading and unloading does not exhibit substantial energy dissipation and that the actual cartilage viscolelastic response takes much longer then are the typical physiological loading durations [131]. Also experimental experience with impact cartilage loading lead to conclusion, that at low rates mechanical behaviour of the tissue was dominated by

fluid exudation, whereas at high loading rates the matrix behaved as an elastic solid with no contribution from fluid flow [23]. In addition, evaluation of compressive energy dissipation in hyaline cartilage was shown to be dependent on loading frequency, peaking at the lowest examined frequency 0.1 Hz in [40]. According to our experience, the higher is the loading rate the lower is the value of dissipated energy (Fig. 16, p. 39). Still we would not regard the lost energy at rapid loading as negligible, as it represents specific damping role of articular cartilage, especially at physiological loading rates. We have also observed, that restoration of original cartilage properties took in general more than ten seconds, but under unconfined compression which is rather distinct from organization inside the joint.

Some authors contribute major role in energy dissipation within articular cartilage to shear stress, as they claim that interstitial fluid flow plays a negligible role in tissue's mechanical response [121]. Osteoarthritic cartilage was found to be more compliant in shear [132], human tibial cartilage has shown significant decrease of dynamic shear modulus with even mild deterioration [69] and also in animal model substantial decrease in dynamic shear modulus with osteoarthritic deterioration was found [29]. These results were concluded to show an increased inter-molecular frictional dissipation due to loosening of collagen-proteoglycan solid matrix. Increased energy losses in impaired articular cartilage can thus be contributed to both of the mechanisms – increased interstitial fluid flow and increased friction between solid matrix components. This only approves the high informative value of dissipated energy in cartilage status assessment.

Quite paradoxically, in this way deterioration of cartilage integrity can be viewed to issue more effective damping; thus even a thin layer of altered cartilage is able to effectively damp applied stress. Moreover, the thinner the cartilage (presumably the more altered is its internal structure) the more energy it absorbs per unit volume (Fig. 32, p. 52). Unfortunately, altered cartilage integrity and composition has a sequel as well in loss of matrix elasticity and thus reversibility of its mechanical performance. As quite substantial time interval would be necessary for damaged cartilage to restore its damping capacity, it does no longer sustain its mechanical function.

4.5 Quantitative features of loading diagrams in automatized characterizing of cartilages in blunt impact testing

In previous section, dissipated energy and related values were found to be related to histological as well as macroscopic cartilage condition. Relations of remaining evaluated quantities to objective findings were not found to be significant. As explained before, loading diagram contains more information than slope and area of hysteresis loop, which were in principle the only used for calculation of biomechanical characteristics.

Specific details of impairment can have specific consequence for the shape of loading diagram. Further features mathematically describing loading curve, even though they do not necessarily have mechanical or physiological foundation, can be helpful in cartilage status classification. Presented results show that seventeen of tested features were found significant for at least one of the histological scores. We have identified some very promising features, such as "Area under 1st third of upwards curve" which seems to be significant for all the scores examined. The most of the features usable (with statistical significance) for distinguishing between samples of different quality was found for score II - – total 13 features. For score I, V and VI there were only 2–3 features for each score, and for score III only one feature was identified as statistically significant.

Based on these result it was revealed, that it is possible to build up a decision tree consisting of combination of up to six mathematical criteria specific for each of the scores, that would be able correctly predict (probability $> 95\,\%$) histological status according to measured loading diagram. Notable advantage of introduced data processing method is that it makes use of the whole set of measured data.

As the decisive algorithms were constructed using presented data, further evaluation on independent set of data is required. Still this appears to be a promising approach for automatized, evidence based decision making concerning articular status condition.

4.6 Impact testing method in tensile examination of ligaments and tendons

The critical factor in a successful anterior cruciate ligament (ACL) reconstruction is the graft choice. Its biomechanical properties strongly influence the surgeon's preference [75, 133]. There are many individual factors that can affect the results of an ACL reconstruction, such as pretensioning of the graft, tensioning and fixation devices used. Multiple-strand hamstring-tendon grafts have become an increasingly popular choice for reconstruction of the anterior cruciate ligament when the use of patellar ligament grafts is associated with recognized donor-site morbidity [73, 134]. The results of our study demonstrate that equally tensioned four-strand hamstring-tendon grafts have higher ultimate tensile strength than those in other varieties of samples tested. From the biomechanical point of view, they seem to be a reasonable alternative procedure for ACL reconstruction.

Such a conclusion is based on presented novel dynamic strain evaluation of the grafts. The grafts are commonly of complicated composite structure with nonlinear responses to loading. Therefore, the aim of the experiments was to determine whether shock testing can be used to characterize their dynamic mechanical proper-

ties. The method of drop-weight testing was proposed, simulating the impact actuation of bioelement under conditions similar to those in natural circumstances. Consequently, the maximum strength values obtained experimentally can be exploited to define the marginal conditions for the robustness of the substance in the case of its injury.

The mechanical behavior of two types of hamstring grafts was compared in presented study, including impact dynamic loading and tensile load-to-failure. Hamstrings – both gracilis and semitendinosus – were measured as single, and also double strands (when they were looped over the upper wedge in the upper clamp). The same combination of double loops of gracilis and semitendinosus was adapted for quadruple strand measurement. Both free-end pairs of the tendons were secured in the lower clamp. All the strands were tensioned equally during the clamping process. In our opinion this procedure resulted in equal tension on each strand. This concern was also applied to evenly load the gracilis and semitendinosus strands when the lower clamp was tightened. In all cases equal tension was maintained by gravitation and the weight of the metal holder for the lower clamp. In the tests the tension was applied with the drop-weight acting at the lower end of all types of strands. The proper clamping of the tissue material may be the priority factor for the correct interpretation of the measured results. The major advantage of the wedge-action grips used in our experiments is that they allow continual adjustment of the clamping pressure with only slight distortion of the compressed tissues between each surface of bi-sided clamp. Thus, there is lesser chance of failure at the clamp-tendon interface. In addition, the use of the sandpaper interface as a gripping technique for soft tissue mechanical testing is adequate in providing consistent and accurate results. The exact tensile strength and stiffness of the graft can only be measured if the specimen fails between the upper and lower clamps. If a tear appears at the fixing point, the measurement is not considered to be relevant.

Noyes [71] and Hamner [75] with coworkers deeply studied the biomechanical properties of ACL substitutes. Both groups confirmed that a four-strand semitendinosus and gracilis graft can have 250 % of the stiffness of the original ACL. Our laboratory study explains it and clearly proves that the strength and stiffness of a combined four-strand hamstring graft is stronger and stiffer than either a ten-millimeter patellar ligament graft or the original ACL specimen.

The bone-patellar tendon-bone autograft is often the first choice for revision anterior cruciate surgery. Good alternative for revision surgery should be autologous hamstring grafts. The use of hamstring grafts reduces the high failure rate after anterior cruciate allograft revision surgery [73, 135].

5 Conclusion

Needs listed in the introduction part (sections 1.8, 1.9) induced construction of a novel device for mechanical characterization of native and tissue-engineered cartilage samples. Developed impact testing method is based on pendulum setup. Samples are loaded dynamically, in direction normal to their surface. Impactor body strikes horizontally the specimen, while the deformation data are read in the axis of deformation using piezoelectric accelerometer and laser doppler vibrometer. This design was shown to be very effective. The whole measurement procedure, from sample attachment to saving acquired data, lasts only a few seconds. Yielded information comprehensively characterizes examined samples under specific desired conditions – loading rates and stresses resembling physiological loading. Gained acceleration/velocity time course is then computationally processed and finally provides loading diagrams and values of well defined mechanical quantities. Attachment of samples was projected with respect to their nature, thus it is easy to handle. Reliability and reproducibility of measurements were assured by repeated measurements of different materials. Resulting data reflected different material properties. Repeated measurements of single sample as well as of different corresponding samples showed reasonable variance. Increased variance in subsequent experiments was conditioned mainly by slightly varying shape of samples. Efforts to suppress this variance was partially limited regarding native tissue, as examination of specimens with natural surface was intended.

The designed method was employed in comparative studies as well as in quantitative evaluation of mechanical parameters, regarding native and artificial cartilage tissue.

Considering native tissue, firstly samples from the non-weight bearing zone (treated as intact) and samples from defect zone were compared. No differences in ultimate quantities were found. On the other hand, significant differences in stiffness and tangent modulus at lower loadings were proved. Impaired tissue showed substantial decrease in both stiffness and modulus values. The fact that tissue degradation is accompanied by decline of its mechanical quality is in coincidence with previously published findings exploiting different methodologies.

In broader study, involving samples from four different cartilage locations within the knee joint, mechanical characteristics were matched to objective histological and macroscopical findings. The revealed relationship of stiffness and modulus to cartilage condition was not found significant. This fact is caused by large variance of acquired results. The large variance is then contributed to three main factors: (i) variation of considered quantities with location within the knee joint cartilage, (ii) uneven sample surface and eventual difficulties in shape determination in native samples, (iii) not all degenerative changes have to necessarily bring the same biomechanical conse-

quences – this can be demonstrated by the loading diagrams in Fig. 20 (p. 42) and Fig. 26 (p. 49). In contrary, dissipated energy and derived quantities were found to be an unambiguous mechanical characteristic of cartilage condition. Decreased cartilage quality has always caused an increase in energy dissipation. Dissipated energy values correlated significantly with both histological and macroscopical cartilage quality classifications. Dissipated energy was so far a neglected feature in cartilage quality assessment. According to our findings its relevance should be emphasized. Consideration of the dissipated energy as a diagnostic marker is suggested. Measurements focused on quality of different tissue-engineered scaffolds for implantation of autologous chondrocytes lead to several conclusions. Woven and knitted scaffolds of biodegradable fibers were examined, some of them (e.g. Chirlac fibers) revealing suitable mechanical properties. Fibrin scaffolds, which are used in routine practice in human medicine, have been found to improve their mechanical properties when controlled solidification was run during their preparation. Fibrin scaffolds enriched with different amount of collagen and hyaluronate were compared, consequently the one best resembling native tissue was chosen for further research. Biomechanical parameters of enriched graft were found to be more suitable than those of pure fibrin graft. This scaffold can be according to *in vivo* tests suggested for routine practice. Different approaches of scaffold modification were confirmed to affect its mechanical response. Thus, introduced testing method was found to be a valuable tool for quality assessment of both artificial and native cartilage, as well as for their mutual comparison.

Analogous measurement principle was employed as well for dynamic tensile testing. Results have revealed differences in mechanical properties between anterior cruciate ligament and grafts used as its autologous substitutes.

Mechanical properties of implanted chondrografts after their incorporation *in vivo* would be also of particular interest. Such material is unfortunately usually not available. In animal studies primary interest is payed to their histological and biological features, thus the lack of samples for mechanical examination. In human autologous chondrocytes implantations non-invasive follow-up is carried out. Though this approach does not directly determine mechanical properties of implants, it informs about cartilage regeneration in general. Database environment was created to facilitate clinical data collection (Fig. 36). Gathered results proved outstanding restoration level of articular cartilage after autologous chondrocyte implantation using fibrin scaffolds (e.g. [16]). This implies satisfactory mechanical quality of used grafts even after their incorporation.

Recent activities in described field are concentrated on data processing. As it is quite uneasy to define a universal suitable quantity to describe mechanical properties of tested materials, more general approach could be beneficial. Complex evaluation of

mathematical characteristics of loading diagrams appears to be a promising method. So far it was found to be feasible to find several diagram features for decisive sorting of native cartilage samples, which gives results corresponding to histological classification.

Designed measurement apparatus and data processing mechanism is under continuous development, today aiming especially to suppressing the influence of sample geometry on acquired data.

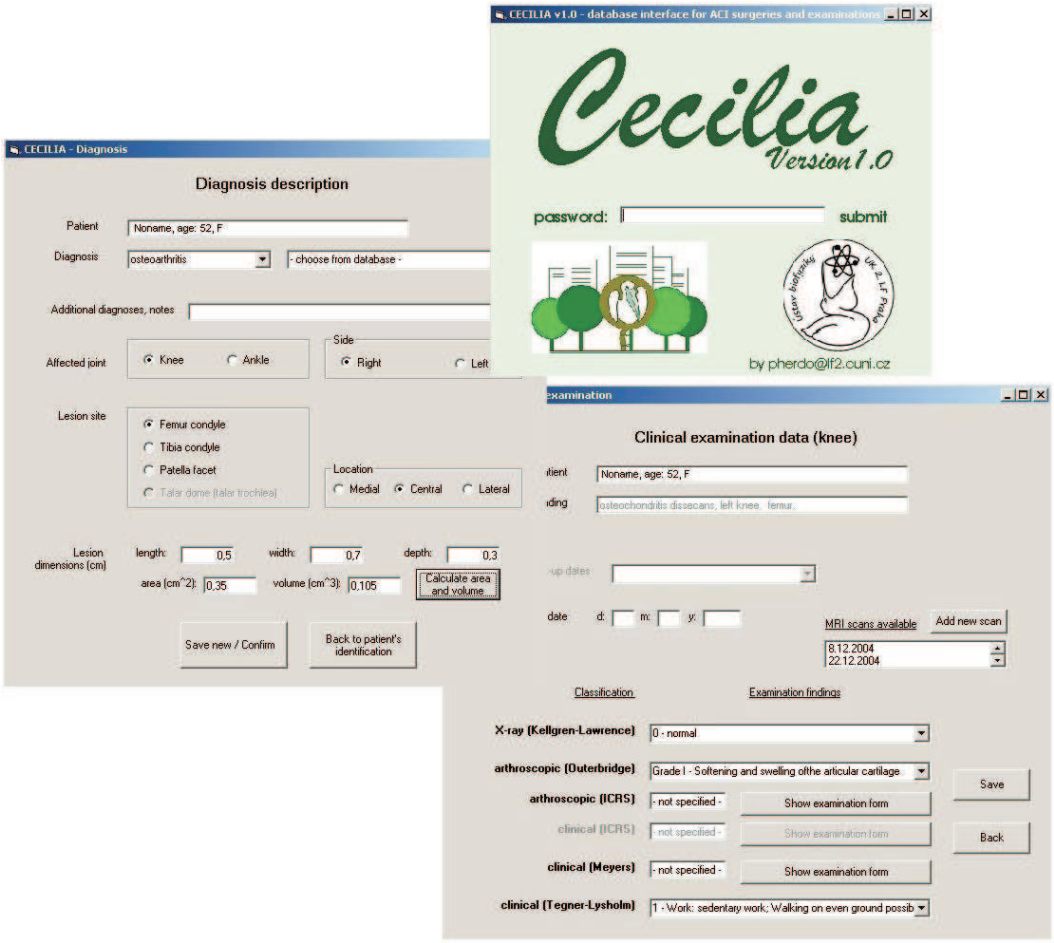

Figure 36: Database environment for follow-up of patients with implantated autologous chondrocytes.

References

[1] VC Mow and LA Setton. In KD Brandt, M Doherty, and LS Lohmander, editors, *Osteoarthritis*, chapter Mechanical Properties of Normal and Osteoarthritic Articular Cartilage, pages 108–122. Oxford University Press, 1998.

[2] VC Mow, A Ratcliffe, and AR Poole. Cartilage and diarthrodial joints as paradigms for hierarchical materials and structures. *BIOMATERIALS*, 13(2):67–97, 1992.

[3] JA Buckwalter and HJ Mankin. Articular cartilage. 1. Tissue design and chondrocyte-matrix interactions. *JOURNAL OF BONE AND JOINT SURGERY-AMERICAN VOLUME*, 79A(4):600–611, APR 1997.

[4] EM Darling and KA Athanasiou. Articular cartilage: Bioreactors and bioprocesses. *TISSUE ENGINEERING*, 9(1):9–26, FEB 2003.

[5] AC Hall, ER Horwitz, and RJ Wilkins. The cellular physiology of articular cartilage. *EXPERIMENTAL PHYSIOLOGY*, 81(3):535–545, MAY 1996.

[6] MA Adams, AK Merrill, and Kerin AJ. Mechanically induced proteoglycan loss from damaged articular cartilage in-vitro. *TRANSACTIONS OF ORTHOPAEDIC RESEARCH SOCIETY*, pages 403–409, 1997.

[7] JA Buckwalter and HJ Mankin. Articular cartilage: Degeneration and osteoarthritis, repair, regeneration, and transplantation. In Cannon, WD, editor, *INSTRUCTIONAL COURSE LECTURES, VOL 47 - 1998*, volume 47 of *AMERICAN ACADEMY OF ORTHOPAEDIC SURGEONS INSTRUCTIONAL COURSE LECTURES*, pages 487–504, 1998. American-Academy-of-Orthopaedic-Surgeons, SAN FRANCISCO, CA, FEB 13-17, 1997.

[8] EB Hunziker. Articular cartilage repair: basic science and clinical progress. A review of the current status and prospects. *OSTEOARTHRITIS AND CARTILAGE*, 10(6):432–463, JUN 2002.

[9] J. Szivek, CL Bliss, CP Geffre, DS Margolis, DW DeYoung, JT Ruth, AB Schnepp, BC Tellis, and RK Vaidyanathan. An instrumented scaffold can monitor loading in the knee joint. *JOURNAL OF BIOMEDICAL MATERIALS RESEARCH PART B-APPLIED BIOMATERIALS*, 79B(2):218–228, NOV 2006.

[10] L Peterson, M Brittberg, I Kiviranta, EL Akerlund, and A Lindahl. Autologous chondrocyte transplantation - Biomechanics and long-term durability. *AMERICAN JOURNAL OF SPORTS MEDICINE*, 30(1):2–12, JAN-FEB 2002.

[11] C Cooper, T McAlindon, D Coggon, P Egger, and P Dieppe. Occupational activity and osteoarthritis of the knee. *ANNALS OF THE RHEUMATIC DISEASES*, 53(2):90–93, FEB 1994.

[12] P Cherubino, FA Grassi, P Bulgheroni, and M Ronga. Autologous chondrocyte implantation using a bilayer collagen membrane: a preliminary report. *JOURNAL OF ORTHOPAEDIC SURGERY (Hong Kong)*, 11:10–15, 2003.

[13] S Marlovits, P Zeller, P Singer, C Resinger, and V Vecsei. Cartilage repair: Generations of autologous chondrocyte transplantation. *EUROPEAN JOURNAL OF RADIOLOGY*, 57(1):24–31, JAN 2006.

[14] GA Ameer, TA Mahmood, and R Langer. A biodegradable composite scaffold for cell transplantation. *JOURNAL OF ORTHOPAEDIC RESEARCH*, 20(1):16–19, JAN 2002.

[15] GP Chen, T Sato, T Ushida, R Hirochika, Y Shirasaki, N Ochiai, and T Tateishi. The use of a novel PLGA fiber/collagen composite web as a scaffold for engineering of articular cartilage tissue with adjustable thickness. *JOURNAL OF BIOMEDICAL MATERIALS RESEARCH PART A*, 67A(4):1170–1180, DEC 15 2003.

[16] M Handl, T Trc, M Hanus, E Stastny, M Fricova-Poulova, J Neuwirth, J Adler, D Havranova, and F Varga. Autologous chondrocyte implantation in the treatment of cartilage lesions of ankle joint. *ACTA CHIRURGIAE ORTHOPAEDICAE ET TRAUMATOLOGIAE CECHOSLOVACA*, 74(1):29–36, FEB 2007.

[17] DL Butler, SA Goldstein, and F Guilak. Functional tissue engineering: The role of biomechanics. *JOURNAL OF BIOMECHANICAL ENGINEERING-TRANSACTIONS OF THE ASME*, 122(6):570–575, DEC 2000.

[18] G Bergmann, G Deuretzbacher, M Heller, F Graichen, A Rohlmann, J Strauss, and GN Duda. Hip contact forces and gait patterns from routine activities. *JOURNAL OF BIOMECHANICS*, 34(7):859–871, JUL 2001.

[19] LV Burgin and RM Aspden. A drop tower for controlled impact testing of biological tissues. *MEDICAL ENGINEERING & PHYSICS*, 29(4):525–530, MAY 2007.

[20] RM Aspden, JE Jeffrey, and LV Burgin. Impact loading: physiological or pathological? *OSTEOARTHRITIS AND CARTILAGE*, 10(7):588–589, JUL 2002.

[21] RU Repo and JB Finlay. Survival of articular-cartilage after controlled impact. *JOURNAL OF BONE AND JOINT SURGERY-AMERICAN VOLUME*, 59(8):1068–1076, 1977.

[22] JJ Garcia, NJ Altiero, and RC Haut. An approach for the stress analysis of transversely isotropic biphasic cartilage under impact load. *JOURNAL OF BIOMECHANICAL ENGINEERING-TRANSACTIONS OF THE ASME*, 120(5):608–613, OCT 1998.

[23] LV Burgin and RM Aspden. Impact testing to determine the mechanical properties of articular cartilage in isolation and on bone. *JOURNAL OF MATERIALS SCIENCE-MATERIALS IN MEDICINE*, 19(2):703–711, FEB 2008.

[24] A Verteramo and BB Seedhom. Effect of a single impact loading on the structure and mechanical properties of articular cartilage. *JOURNAL OF BIOMECHANICS*, 40(16):3580–3589, 2007.

[25] FH Silver and G Bradica. Mechanobiology of cartilage: how do internal and external stresses affect mechanochemical transduction and elastic energy storage? *BIOMECHANICS AND MODELING IN MECHANOBIOLOGY*, 1:219–238, 2002.

[26] T Gibson and WB Davis. The distortion of autologous cartilage grafts: its cause and prevention. *BRITISH JOURNAL OF PLASTIC SURGERY*, 10:257–274, 1958.

[27] WM Lai, JS Hou, and VC Mow. A triphasic theory for the swelling and deformation behaviors of articular-cartilage. *JOURNAL OF BIOMECHANICAL ENGINEERING-TRANSACTIONS OF THE ASME*, 113(3):245–258, AUG 1991.

[28] PA Torzilli. Influence of cartilage conformation on its equilibrium water partition. *JOURNAL OF ORTHOPAEDIC RESEARCH*, 3(4):473–483, 1985.

[29] LA Setton, DM Elliott, and VC Mow. Altered mechanics of cartilage with osteoarthritis: human osteoarthritis and an experimental model of joint degeneration. *OSTEOARTHRITIS AND CARTILAGE*, 7(1):2–14, JAN 1999.

[30] P Kelly. Solid mechanics: Part 1 – an introduction to solid mechanics. chapter Viscoelasticity, pages 233–292. 2008.

[31] CW McCutchen. Cartilage is poroelastic, not viscoelastic (including an exact theorem about strain-energy and viscous loss, and an order of magnitude relation for equilibration time). *JOURNAL OF BIOMECHANICS*, 15(4):325–327, 1982.

[32] NG Shrive and Frank CB. In BM Nigg and W Herzog, editors, *Biomechanics of the Musculo-Skeletal System*, chapter Articular Cartilage, pages 86–106. John Wiley, 1999.

[33] GA Ateshian, WH Warden, JJ Kim, RP Grelsamer, and VC Mow. Finite deformation biphasic material properties of bovine articular cartilage from confined compression experiments. *JOURNAL OF BIOMECHANICS*, 30(11-12):1157–1164, NOV-DEC 1997.

[34] M Fortin, J Soulhat, A Shirazi-Adl, EB Hunziker, and MD Buschmann. Unconfined compression of articular cartilage: Nonlinear behavior and comparison with a fibril-reinforced biphasic model. *JOURNAL OF BIOMECHANICAL ENGINEERING-TRANSACTIONS OF THE ASME*, 122(2):189–195, APR 2000.

[35] MK Barker and BB Seedhom. The relationship of the compressive modulus of articular cartilage with its deformation response to cyclic loading: does cartilage optimize its modulus so as to minimize the strains arising in it due to the prevalent loading regime? *RHEUMATOLOGY*, 40(3):274–284, MAR 2001.

[36] W Grellmann, A Berghaus, EJ Haberland, Y Jamali, K Holweg, K Reincke, and C Bierogel. Determination of strength and deformation behavior of human cartilage for the definition of significant parameters. *JOURNAL OF BIOMEDICAL MATERIALS RESEARCH PART A*, 78A(1):168–174, JUL 2006.

[37] RL Mauck, MA Soltz, CCB Wang, DD Wong, PHG Chao, WB Valhmu, CT Hung, and GA Ateshian. Functional tissue engineering of articular cartilage through dynamic loading of chondrocyte-seeded agarose gels. *JOURNAL OF BIOMECHANICAL ENGINEERING-TRANSACTIONS OF THE ASME*, 122(3):252–260, JUN 2000. Bioengineering Conference, BIG SKY, MONTANA, JUN 16-20, 1999.

[38] V Musahl, SD Abramowitch, MT Gabriel, RE Debski, P Hertel, FH Fu, and SLY Woo. Tensile properties of an anterior cruciate ligament graft after bone-patellar tendon-bone press-fit fixation. *KNEE SURGERY SPORTS TRAUMATOLOGY ARTHROSCOPY*, 11(2):68–74, MAR 2003.

[39] MK Barker and BB Seedhom. Articular cartilage deformation under physiological cyclic loading-apparatus and measurement technique. *JOURNAL OF BIOMECHANICS*, 30(4):377–381, APR 1997.

[40] S Miyata, T Tateishi, K Furukawa, and T Ushida. Influence of structure and composition on dynamic viscoelastic property of cartilaginous tissue: Criteria for classification between hyaline cartilage and fibrocartilage based on mechanical function. *JSME INTERNATIONAL JOURNAL SERIES C-MECHANICAL SYSTEMS MACHINE ELEMENTS AND MANUFACTURING*, 48(4):547–554, DEC 2005.

[41] T Lyyra-Laitinen, M Niinimaki, J Toyras, R Lindgren, I Kiviranta, and JS Jurvelin. Optimization of the arthroscopic indentation instrument for the measurement of thin cartilage stiffness. *PHYSICS IN MEDICINE AND BIOLOGY*, 44(10):2511–2524, OCT 1999.

[42] WC Bae, MA Temple, D Amiel, RD Coutts, GG Niederauer, and RL Sah. Indentation testing of human cartilage - Sensitivity to articular surface degeneration. *ARTHRITIS AND RHEUMATISM*, 48(12):3382–3394, DEC 2003.

[43] RK Korhonen, S Saarakkala, J Toyras, MS Laasanen, K Kiviranta, and JS Jurvelin. Experimental and numerical validation for the novel configuration of an arthroscopic indentation instrument. *PHYSICS IN MEDICINE AND BIOLOGY*, 48(11):1565–1576, JUN 7 2003.

[44] T Lyyra, J Jurvelin, P Pitkanen, U Vaatainen, and I Kiviranta. Indentation instrument for the measurement of cartilage stiffness under arthroscopic control. *MEDICAL ENGINEERING & PHYSICS*, 17(5):395–399, JUL 1995.

[45] RC Appleyard, MV Swain, S Khanna, and GAC Murrell. The accuracy and reliability of a novel handheld dynamic indentation probe for analysing articular cartilage. *PHYSICS IN MEDICINE AND BIOLOGY*, 46(2):541–550, FEB 2001.

[46] T Franz, EM Hasler, R Hagg, C Weiler, RP Jakob, and P Mainil-Varlet. In situ compressive stiffness, biochemical composition, and structural integrity of articular cartilage of the human knee joint. *OSTEOARTHRITIS AND CARTILAGE*, 9(6):582–592, AUG 2001.

[47] GG Niederauer, GM Niederauer, LC Cullen, KA Athanasiou, JB Thomas, and MQ Niederauer. Correlation of cartilage stiffness to thickness and level of degeneration using a handheld indentation probe. *ANNALS OF BIOMEDICAL ENGINEERING*, 32(3):352–359, MAR 2004.

[48] MS Laasanen, J Toyras, RK Korhonen, J Rieppo, S Saarakkala, MT Nieminen, J Hirvonen, and JS Jurvelin. Biomechanical properties of knee articular cartilage. *BIORHEOLOGY*, 40(1-3, Sp. Iss. SI):133–140, 2003. FRANCE, APR 24-26, 2001.

[49] JKF Suh, I Youn, and FH Fu. An in situ calibration of an ultrasound transducer: a potential application for an ultrasonic indentation test of articular cartilage. *JOURNAL OF BIOMECHANICS*, 34(10):1347–1353, OCT 2001.

[50] MH Lu, YP Zheng, QH Huang, C Ling, Q Wang, L Bridal, L Qin, and A Mak. Noncontact Evaluation of Articular Cartilage Degeneration Using a Novel Ultrasound Water Jet Indentation System. *ANNALS OF BIOMEDICAL ENGINEERING*, 37(1):164–175, JAN 2009.

[51] Zaifeng Fan, Peter A. Smith, Eugene C. Eckstein, and Gerald F. Harris. Mechanical properties of OI type III bone tissue measured by nanoindentation. *JOURNAL OF BIOMEDICAL MATERIALS RESEARCH PART A*, 79A(1):71–77, OCT 2006.

[52] J Norman, JG Shapter, K Short, LJ Smith, and NL Fazzalari. Micromechanical properties of human trabecular bone: A hierarchical investigation using nanoindentation. *JOURNAL OF BIOMEDICAL MATERIALS RESEARCH PART A*, 87A(1):196–202, OCT 2008.

[53] G Pelled, K Tai, D Sheyn, Y Zilberman, S Kumbar, LS Nair, CT Laurencin, D Gazit, and C Ortiz. Structural and nanoindentation studies of stem cell-based tissue-engineered bone. *JOURNAL OF BIOMECHANICS*, 40(2):399–411, 2007.

[54] O Franke, K Durst, V Maier, M Goken, T Birkhoiz, H Schneider, F Hennig, and K Gelse. Mechanical properties of hyaline and repair cartilage studied by nanoindentation. *ACTA BIOMATERIALIA*, 3(6):873–881, NOV 2007.

[55] C Li, LA Pruitt, and KB King. Nanoindentation differentiates tissue-scale functional properties of native articular cartilage. *JOURNAL OF BIOMEDICAL MATERIALS RESEARCH PART A*, 78A(4):729–738, SEP 15 2006.

[56] DM Ebenstein, A Kuo, JJ Rodrigo, AH Reddi, M Ries, and L Pruitt. A nanoindentation technique for functional evaluation of cartilage repair tissue. *JOURNAL OF MATERIALS RESEARCH*, 19(1):273–281, JAN 2004.

[57] J Xu, JY Rho, SR Mishra, and Z Fan. Atomic force microscopy and nanoindentation characterization of human lamellar bone prepared by microtome sectioning

and mechanical polishing technique. *JOURNAL OF BIOMEDICAL MATERIALS RESEARCH PART A*, 67A(3):719–726, DEC 1 2003.

[58] S Park, KD Costa, GA Ateshian, and KS Hong. Mechanical properties of bovine articular cartilage under microscale indentation loading from atomic force microscopy. *PROCEEDINGS OF THE INSTITUTION OF MECHANICAL ENGINEERS PART H-JOURNAL OF ENGINEERING IN MEDICINE*, 223(H3):339–347, APR 2009.

[59] K Hattori, K Mori, T Habata, Y Takakura, and K Ikeuchi. Measurement of the mechanical condition of articular cartilage with an ultrasonic probe: quantitative evaluation using wavelet transformation. *CLINICAL BIOMECHANICS*, 18(6):553–557, JUL 2003.

[60] H Kuroki, Y Nakagawa, K Mori, M Kobayashi, K Yasura, Y Okamoto, T Suzuki, K Nishitani, and T Nakamura. Ultrasound properties of articular cartilage in the tibio-femoral joint in knee osteoarthritis: relation to clinical assessment (International Cartilage Repair Society grade). *ARTHRITIS RESEARCH & THERAPY*, 10(4), 2008.

[61] SI Berkenblit, EH Frank, EP Salant, and AJ Grodzinsky. Nondestructive detection of cartilage degeneration using electromechanical surface spectroscopy. *JOURNAL OF BIOMECHANICAL ENGINEERING-TRANSACTIONS OF THE ASME*, 116(4):384–392, NOV 1994.

[62] JR Sachs and AJ Grodzinsky. Electromechanical spectroscopy of cartilage using a surface probe with applied mechanical displacement. *JOURNAL OF BIOMECHANICS*, 28(8):963–976, AUG 1995.

[63] JH Dashefsky. Arthroscopic measurement of chondromalacia of patella cartilage using a microminiature pressure transducer. *ARTHROSCOPY*, 3:80–85, 1987.

[64] PS Donzelli, RL Spilker, GA Ateshian, and VC Mow. Contact analysis of biphasic transversely isotropic cartilage layers and correlations with tissue failure. *JOURNAL OF BIOMECHANICS*, 32(10):1037–1047, OCT 1999.

[65] XW Li, RC Haut, and NJ Altiero. An analytical model to study blunt impact response of the rabbit P-F joint. *JOURNAL OF BIOMECHANICAL ENGINEERING-TRANSACTIONS OF THE ASME*, 117(4):485–491, NOV 1995.

[66] AJ Kerin, MR Wisnom, and MA Adams. The compressive strength of articular cartilage. *PROCEEDINGS OF THE INSTITUTION OF MECHANICAL ENGINEERS PART H-JOURNAL OF ENGINEERING IN MEDICINE*, 212(H4):273–280, 1998.

[67] LV Burgin and RM Aspden. Impact loading of human articular cartilage. *JOURNAL OF BIOMECHANICS (Abstracts)*, 34:S39–S40, 2001.

[68] G Bellucci and BB Seedhom. Mechanical behaviour of articular cartilage under tensile cyclic load. *RHEUMATOLOGY*, 40(12):1337–1345, DEC 2001.

[69] AA Young, RC Appleyard, MM Smith, J Melrose, and CB Little. Dynamic biomechanics correlate with histopathology in human tibial cartilage. *CLINICAL ORTHOPAEDICS AND RELATED RESEARCH*, (462):212–220, SEP 2007.

[70] DL Butler, ES Grood, FR Noyes, RF Zernicke, and K Brackett. Effects of structure and strain-measurement technique on the material properties of young human tendons and fascia. *JOURNAL OF BIOMECHANICS*, 17(8):579–596, 1984.

[71] FR Noyes, DL Butler, ES Grood, RF Zernicke, and MS Hefzy. Biomechanical analysis of human ligament grafts used in knee-ligament repairs and reconstructions. *JOURNAL OF BONE AND JOINT SURGERY-AMERICAN VOLUME*, 66A(3):344–352, 1984.

[72] FT Blevins, AT Hecker, GT Bigler, AL Boland, and WC Hayes. The effects of donor age and strain-rate on the biomechanical properties of bone-patellar tendon-bone allografts. *AMERICAN JOURNAL OF SPORTS MEDICINE*, 22(3):328–333, MAY-JUN 1994.

[73] FR Noyes and SD Barber-Westin. Revision anterior cruciate surgery with use of bone-patellar tendon-bone autogenous grafts. *JOURNAL OF BONE AND JOINT SURGERY-AMERICAN VOLUME*, 83A(8):1131–1143, AUG 2001.

[74] M Kurosaka, S Yoshiya, and JT Andrish. A biomechanical comparison of different surgical techniques of graft fixation in anterior cruciate ligament reconstruction. *AMERICAN JOURNAL OF SPORTS MEDICINE*, 15(3):225–229, MAY-JUN 1987.

[75] DL Hamner, CH Brown, ME Steiner, AT Hecker, and WC Hayes. Hamstring tendon grafts for reconstruction of the anterior cruciate ligament: Biomechanical evaluation of the use of multiple strands and tensioning techniques. *JOURNAL*

OF BONE AND JOINT SURGERY-AMERICAN VOLUME, 81A(4):549–557, APR 1999.

[76] ZA Cohen, DM McCarthy, SD Kwak, P Legrand, F Fogarasi, EJ Ciaccio, and GA Ateshian. Knee cartilage topography, thickness, and contact areas from MRI: in-vitro calibration and in-vivo measurements. *OSTEOARTHRITIS AND CARTILAGE*, 7(1):95–109, JAN 1999.

[77] Y Xia, JB Moody, N Burton-Wurster, and G Lust. Quantitative in situ correlation between microscopic MRI and polarized light microscopy studies of articular cartilage. *OSTEOARTHRITIS AND CARTILAGE*, 9(5):393–406, JUL 2001.

[78] J Mollenhauer, ME Aurich, Z Zhong, C Muehleman, CC Cole, M Hasnah, O Oltulu, KE Kuettner, A Margulis, and LD Chapman. Diffraction-enhanced X-ray imaging of articular cartilage. *OSTEOARTHRITIS AND CARTILAGE*, 10(3):163–171, MAR 2002.

[79] MJ Nissi, J Toyras, MS Laasanen, J Rieppo, S Saarakkala, R Lappalainen, JS Jurvelin, and MT Nieminen. Proteoglycan and collagen sensitive MRI evaluation of normal and degenerated articular cartilage. *JOURNAL OF ORTHOPAEDIC RESEARCH*, 22(3):557–564, MAY 2004.

[80] RE Outerbridge. The etiology of chondromalacia patellae. *JOURNAL OF BONE AND JOINT SURGERY-BRITISH VOLUME*, 43(4):752–757, 1961.

[81] P Mainil-Varlet, T Aigner, M Brittberg, P Bullough, A Hollander, E Hunziker, R Kandel, S Nehrer, K Pritzker, S Roberts, and E Stauffer. Histological assessment of cartilage repair - A report by the Histology Endpoint Committee of the International Cartilage Repair Society (ICRS). *JOURNAL OF BONE AND JOINT SURGERY-AMERICAN VOLUME*, 85A(Suppl. 2):45–57, 2003. 4th Symposium of the International-Cartilage-Repair-Society, TORONTO, CANADA, JUN 15-18, 2002.

[82] HJ Mankin, H Dorfman, L Lippiell, and A Zarnis. Biochemical and metabolic abnormalities in articular cartilage from osteoarthritic human hips. 2: Correlation of morphology with biochemical and metabolic data. *ARTHRITIS AND RHEUMATISM*, 14(3):400–&, 1971.

[83] RC Appleyard, D Burkhardt, P Ghosh, R Read, M Cake, MV Swain, and GAC Murrell. Topographical analysis of the structural, biochemical and dynamic biomechanical properties of cartilage in an ovine model of osteoarthritis. *OSTEOARTHRITIS AND CARTILAGE*, 11(1):65–77, JAN 2003.

[84] SP Oakley, MN Lassere, I Portek, Z Szomor, P Ghosh, BW Kirkham, GAC Murrell, S Wulf, and RC Appleyard. Biomechanical, histologic and macroscopic assessment of articular cartilage in a sheep model of osteoarthritis. *OSTEOARTHRITIS AND CARTILAGE*, 12(8):667–679, AUG 2004.

[85] RU Kleemann, D Krocker, A Cedraro, J Tuischer, and GN Duda. Altered cartilage mechanics and histology in knee osteoarthritis: relation to clinical assessment (ICRS Grade). *OSTEOARTHRITIS AND CARTILAGE*, 13(11):958–963, NOV 2005.

[86] J Arokoski, J Jurvelin, I Kiviranta, M Tammi, and HJ Helminen. Softening of the lateral condyle articular-cartilage in the canine knee-joint after long-distance (up to 40km/day) running training lasting one-year. *INTERNATIONAL JOURNAL OF SPORTS MEDICINE*, 15(5):254–260, JUL 1994.

[87] RC Appleyard, P Ghosh, and MV Swain. Biomechanical, histological and immunohistological studies of patellar cartilage in an ovine model of osteoarthritis induced by lateral meniscectomy. *OSTEOARTHRITIS AND CARTILAGE*, 7(3):281–294, MAY 1999.

[88] GN Duda, A Haisch, M Endres, C Gebert, D Schroeder, JE Hoffmann, and M Sittinger. Mechanical quality of tissue engineered cartilage: Results after 6 and 12 weeks in vivo. *JOURNAL OF BIOMEDICAL MATERIALS RESEARCH*, 53(6):673–677, DEC 5 2000.

[89] Y Chae, G Aguilar, EJ Lavernia, and BJF Wong. Characterization of temperature dependent mechanical behavior of cartilage. *LASERS IN SURGERY AND MEDICINE*, 32(4):271–278, 2003. American-Society-for-Laser-Medicine-and-Surgery, ATLANTA, GEORGIA, APR 11, 2002.

[90] JZ Wu and W Herzog. Elastic anisotropy of articular cartilage is associated with the microstructures of collagen fibers and chondrocytes. *JOURNAL OF BIOMECHANICS*, 35(7):931–942, JUL 2002.

[91] DM Elliott, DA Narmoneva, and LA Setton. Direct measurement of the Poisson's ratio of human patella cartilage in tension. *JOURNAL OF BIOMECHANICAL ENGINEERING-TRANSACTIONS OF THE ASME*, 124(2):223–228, APR 2002.

[92] H Jin and JL Lewis. Determination of Poisson's ratio of articular cartilage by indentation using different-sized indenters. *JOURNAL OF BIOME-*

CHANICAL ENGINEERING-TRANSACTIONS OF THE ASME, 126(2):138–145, APR 2004.

[93] JR Quinlan. Induction of decision trees. *MACHINE LEARNING*, 1:81–106, 1986.

[94] E Filova, M Rampichova, M Handl, A Lytvynets, R Halouzka, D Usvald, J Hlucilova, R Prochazka, M Dezortova, E Rolencova, E Kostakova, T Trc, E Stastny, L Kolacna, M Hajek, J Motlik, and E Amler. Composite hyaluronate-type I collagen-fibrin scaffold in the therapy of osteochondral defects in miniature pigs. *PHYSIOLOGICAL RESEARCH*, 56(Suppl. 1):S5–S16, 2007.

[95] E Filova, F Jelinek, M Handl, A Lytvynets, M Rampichova, F Varga, J Cinatl, T Soukup, T Trc, and E Amler. Novel Composite Hyaluronan/Type I Collagen/Fibrin Scaffold Enhances Repair of Osteochondral Defect in Rabbit Knee. *JOURNAL OF BIOMEDICAL MATERIALS RESEARCH PART B-APPLIED BIOMATERIALS*, 87B(2):415–424, NOV 2008.

[96] M Brittberg and CS Winalski. Evaluation of cartilage injuries and repair. *JOURNAL OF BONE AND JOINT SURGERY-AMERICAN VOLUME*, 85A(Suppl. 2):58–69, 2003. TORONTO, CANADA, JUN 15-18, 2002.

[97] Y Tomita, K Azuma, and M Naito. Computational evaluation of strain-rate-dependent deformation behavior of rubber and carbon-black-filled rubber under monotonic and cyclic straining. *INTERNATIONAL JOURNAL OF MECHANICAL SCIENCES*, 50(5):856–868, MAY 2008. 8th Asia-Pacific Symposium on Advances in Engineering Plasticity and Its Applications (AEPA 2000), Nagoya, JAPAN, SEP, 2006.

[98] JE Jeffrey, DW Gregory, and RM Aapden. Matrix damage and chondrocyte viability following a single impact load on articular-cartilage. *ARCHIVES OF BIOCHEMISTRY AND BIOPHYSICS*, 322(1):87–96, SEP 10 1995.

[99] AP Bovsunovsky. Application of the strain-phase-shift method for the determination of damping in metals. *EXPERIMENTAL MECHANICS*, 36(3):243–250, SEP 1996.

[100] D Low, T Sumii, MV Swain, K Ishigami, and T Takeda. Instrumented indentation characterisation of mouth-guard materials. *DENTAL MATERIALS*, 18(3):211–215, MAY 2002.

[101] I Witten and F Eibe. *Data Mining: Practical machine learning tools and techniques*. 2nd edition, 2005.

[102] VC Mow, SC Kuei, WM Lai, and CG Armstrong. Biphasic creep and stress-relaxation of articular-cartilage in compression – theory and experiments. *JOURNAL OF BIOMECHANICAL ENGINEERING-TRANSACTIONS OF THE ASME*, 102(1):73–84, 1980.

[103] AF Mak. Unconfined compression of hydrated viscoelastic tissues - a biphasic poroviscoelastic analysis. *BIORHEOLOGY*, 23(4):371–383, 1986.

[104] JZ Wu and W Herzog. Finite element simulation of location- and time-dependent mechanical behavior of chondrocytes in unconfined compression tests. *ANNALS OF BIOMEDICAL ENGINEERING*, 28(3):318–330, MAR 2000.

[105] VC Mow, WM Lai, and JS Hou. A triphasic theory for the swelling properties of hydrated charged soft biological tissues. *APPLIED MECHANICS REVIEWS*, 43:134–141, 1990.

[106] L Kolacna, J Bakesova, F Varga, E Kostakova, L Planka, A Necas, D Lukas, E Amler, and V Pelouch. Biochemical and biophysical aspects of collagen nanostructure in the extracellular matrix. *PHYSIOLOGICAL RESEARCH*, 56(Suppl. 1):S51–S60, 2007.

[107] A Oloyede, R Flashmann, and ND Broom. The dramatic influence of loading velocity on the compressive response of articular-cartilage. *CONNECTIVE TISSUE RESEARCH*, 27(4):211–224, 1992.

[108] EMH Obeid, MA Adams, and JH Newman. Mechanical-properties of articular-cartilage in knees with unicompartmental osteoarthritis. *JOURNAL OF BONE AND JOINT SURGERY-BRITISH VOLUME*, 76B(2):315–319, MAR 1994.

[109] R Krishnan, S Park, F Eckstein, and GA Ateshian. Inhomogeneous cartilage properties enhance superficial interstitial fluid support and frictional properties, but do not provide a homogeneous state of stress. *JOURNAL OF BIOMECHANICAL ENGINEERING-TRANSACTIONS OF THE ASME*, 125(5):569–577, OCT 2003.

[110] L Sokoloff. Elasticity of aging cartilage. *FEDERATION PROCEEDINGS*, 25(3P1):1089–1095, 1966.

[111] GE Kempson. Mechanical properties of articular-cartilage. *JOURNAL OF PHYSIOLOGY-LONDON*, 223(1):P23, 1972.

[112] CG Armstrong and VC Mow. Variations in the intrinsic mechanical proterties of human articular-cartilage with age, degeneration, and water-content. *JOURNAL OF BONE AND JOINT SURGERY-AMERICAN VOLUME*, 64(1):88–94, 1982.

[113] KA Athanasiou, A Agarwal, and FJ Dzida. Comparative-study of the intrinsic mechanical-properties of the human acetabular and femoral-head cartilage. *JOURNAL OF ORTHOPAEDIC RESEARCH*, 12(3):340–349, MAY 1994.

[114] RL Sah, AS Yang, AC Chen, JJ Hant, RB Halili, M Yoshioka, D Amiel, and RD Coutts. Physical properties of rabbit articular cartilage after transection of the anterior cruciate ligament. *JOURNAL OF ORTHOPAEDIC RESEARCH*, 15(2):197–203, MAR 1997.

[115] WR Jones, HP Ting-Beall, GM Lee, SS Kelley, RM Hochmuth, and F Guilak. Alterations in the Young's modulus and volumetric properties of chondrocytes isolated from normal and osteoarthritic human cartilage. *JOURNAL OF BIOMECHANICS*, 32(2):119–127, FEB 1999.

[116] P Mainil-Varlet, T Aigner, M Brittberg, P Bullough, A Hollander, E Hunziker, R Kandel, S Nehrer, K Pritzker, S Roberts, and E Stauffer. The International Cartilage Repair Society (ICRS) – Visual histological scale. A preliminary report of the histological end point committee. I. Human biopsies. Toronto consensus. *EUROPEAN CELLS AND MATERIALS*, 4 (Suppl.1):10, 2002.

[117] AC Swann and BB Seedhom. The stiffness of normal articular-cartilage and the predominant acting stress levels - implications for the etiology of osteoarthrosis. *BRITISH JOURNAL OF RHEUMATOLOGY*, 32(1):16–25, JAN 1993.

[118] JQ Yao and BB Seedhom. Mechanical conditioning of articular-cartilage to prevalent stresses. *BRITISH JOURNAL OF RHEUMATOLOGY*, 32(11):956–965, NOV 1993.

[119] DET Shepherd and BB Seedhom. Thickness of human articular cartilage in joints of the lower limb. *ANNALS OF THE RHEUMATIC DISEASES*, 58(1):27–34, JAN 1999.

[120] ND Broom and R Flachsmann. Physical indicators of cartilage health: the relevance of compliance, thickness, swelling and fibrillar texture. *JOURNAL OF ANATOMY*, 202(6):481–494, JUN 2003.

[121] DR Carter, DP Fyhrie, R Whalen, TE Orr, DJ Schurman, and DJ Rapperport. In G Bergmann, R Kolbel, and A Rohlmann, editors, *Biomechanics: Basic and*

Applied Research, chapter Control of chondro-osseous skeletal biology by mechanical energy, pages 219–225. Springer / Martinus Nijhoff Publishers, 1987.

[122] DR Anderson, AP Newman, and AU Daniels. In vitro load transmission in the canine knee: The effect of medial meniscectomy and varus rotation. *KNEE SURGERY, SPORTS TRAUMATOLOGY, ARTHROSCOPY*, 1(1):44–50, Mar 1993.

[123] R Brocklehurst, MT Bayliss, A Maroudas, HL Coysh, MAR Freeman, PA Revell, and SY Ali. The composition of normal and osteoarthritic articular-cartilage from human knee joints - with special reference to unicompartmental replacement and osteotomy of the knee. *JOURNAL OF BONE AND JOINT SURGERY-AMERICAN VOLUME*, 66A(1):95–106, 1984.

[124] EL Radin and RM Rose. Role of subchondral bone in the initiation and progression of cartilage damage. *CLINICAL ORTHOPAEDICS AND RELATED RESEARCH*, (213):34–40, DEC 1986.

[125] H Matsui, M Shimizu, and H Tsuji. Cartilage and subchondral bone interaction in osteoarthrosis of human knee joint: A histological and histomorphometric study. *MICROSCOPY RESEARCH AND TECHNIQUE*, 37(4):333–342, MAY 15 1997.

[126] MAR Freeman. Is collagen fatigue failure a cause of osteoarthrosis and prosthetic component migration? A hypothesis. *JOURNAL OF ORTHOPAEDIC RESEARCH*, 17(1):3–8, JAN 1999.

[127] HJ Mankin and AZ Thrasher. Water-content and binding in normal and osteoarthritic human cartilage. *JOURNAL OF BONE AND JOINT SURGERY-AMERICAN VOLUME*, A 57(1):76–80, 1975.

[128] AJ Bollet and JL Nance. Biochemical findings in normal and osteoarthritic articular cartilage .2. chondroitin sulfate concentration and chain length water and ash content. *JOURNAL OF CLINICAL INVESTIGATION*, 45(7):1170–1177, 1966.

[129] A Maroudas and M Venn. Chemical composition and swelling of normal and osteoarthrotic femoral-head cartilage. 2: Swelling. *ANNALS OF THE RHEUMATIC DISEASES*, 36(5):399–406, 1977.

[130] AW Eberhardt, LM Keer, JL Lewis, and V Vithoontien. An analytical model of joint contact. *JOURNAL OF BIOMECHANICAL ENGINEERING-TRANSACTIONS OF THE ASME*, 112(4):407–413, NOV 1990.

[131] GA Ateshian and CT Hung. In F Guilak, DL Butler, SA Goldstein, and DJ Mooney, editors, *Functional tissue engineering*, chapter Functional properties of native articular cartilage, pages 46–68. Birkhauser, 2003.

[132] WB Zhu, VC Mow, TJ Koob, and DR Eyre. Viscoelastic shear properties of articular-cartilage and the effects of glycosidase treatments. *JOURNAL OF ORTHOPAEDIC RESEARCH*, 11(6):771–781, NOV 1993.

[133] CH Brown, ME Steiner, and EW Carson. The use of hamstring tendons for anterior cruciate ligament reconstruction - technique and results. *CLINICS IN SPORTS MEDICINE*, 12(4):723–756, OCT 1993.

[134] SJ Kim, P Kumar, and KS Oh. Anterior Cruciate Ligament Reconstruction: Autogenous Quadriceps Tendon-Bone Compared With Bone-Patellar Tendon-Bone Grafts at 2-Year Follow-up. *ARTHROSCOPY-THE JOURNAL OF ARTHROSCOPIC AND RELATED SURGERY*, 25(2):137–144, FEB 2009.

[135] FR Noyes, SD Barberwestin, and CS Roberts. Use of allografts after failed treatment of rupture of the anterior cruciate ligament. *JOURNAL OF BONE AND JOINT SURGERY-AMERICAN VOLUME*, 76A(7):1019–1031, JUL 1994.